UHASSELT
KNOWLEDGE IN ACTION

Maastricht University

Faculty of Medicine and Life Sciences
School for Life Sciences
Master of Biomedical Sciences

Master's thesis

Unraveling the Brain's Cleanup Crew: the Role of TRPV4 in Mitochondrial Dynamics during Microglial Phagocytosis

Robin Schellingen

Thesis presented in fulfillment of the requirements for the degree of Master of Biomedical Sciences, specialization Molecular Mechanisms in Health and Disease

SUPERVISOR :

Prof. dr. Bert BRONE

MENTOR :

Mevrouw Elena-Andreea BURLACU

2023
2024

Transnational University Limburg is a unique collaboration of two universities in two countries: the University of Hasselt and Maastricht University.

UHASSELT
KNOWLEDGE IN ACTION

www.uhasselt.be
Universiteit Hasselt
Campus Hasselt:
Martelarenlaan 42 | 3500 Hasselt
Campus Diepenbeek:
Agoralaan Gebouw D | 3590 Diepenbeek

UHASSELT
KNOWLEDGE IN ACTION

Maastricht University

Faculty of Medicine and Life Sciences
School for Life Sciences
Master of Biomedical Sciences

Master's thesis

Unraveling the Brain's Cleanup Crew: the Role of TRPV4 in Mitochondrial Dynamics during Microglial Phagocytosis

Robin Schellingen

Thesis presented in fulfillment of the requirements for the degree of Master of Biomedical Sciences, specialization Molecular Mechanisms in Health and Disease

SUPERVISOR :

Prof. dr. Bert BRONE

MENTOR :

Mevrouw Elena-Andreea BURLACU

Unraveling the Brain's Cleanup Crew: the role of TRPV4 in Mitochondrial Dynamics during Microglial Phagocytosis.

Robin Schellingen[1], Andreea Burlacu[1] and Bert Brône[1]

[1]Morphology research group, Biomedical Research Institute, Universiteit Hasselt, Campus Diepenbeek, Agoralaan Gebouw C - B-3590 Diepenbeek
[2]Physiology research group, Biomedical Research Institute, Universiteit Hasselt, Campus Diepenbeek, Agoralaan Gebouw C - B-3590 Diepenbeek

*Running title: TRPV4's role in microglial mitochondrial dynamics

To whom correspondence should be addressed: Prof. Dr. Bert Brône, Tel: +32 (11) 26 92 37; Email: bert.brone@uhasselt.be

Keywords: Microglia, mitochondrial movement, mitochondria, TRPV4, phagocytosis

ABSTRACT

Microglia, the resident immune cells of the central nervous system (CNS), play a role in maintaining brain homeostasis, with their main function being phagocytosis. The transient receptor potential vanilloid 4 (TRPV4) channel is a cation channel involved in calcium homeostasis, influencing microglial morphology and function. During phagocytosis, a phagocytic cup is formed, which is heavily dependent on cytoskeletal reorganization. This requires energy to facilitate movement of the cell, which is delivered by mitochondria. However, the typical movement of mitochondria during microglial phagocytosis remains elusive. In this study, the role of TRPV4 in mitochondrial dynamics during microglial phagocytosis was evaluated. Using wild-type (WT) and TRPV4 knockout (KO) primary microglia, we assessed mitochondrial distribution and dynamics through immunohistochemistry and live-cell imaging. Our results demonstrate that TRPV4 activity regulates mitochondrial dynamics and distribution. Specifically, TRPV4 KO microglia exhibit a more dispersed mitochondrial distribution and increased mitochondrial fission compared to WT microglia. We prove that acute inhibition of TRPV4 with a specific TRPV4 antagonist directly affects mitochondrial dynamics in WT microglia, indicative of increased mitochondrial fission. The increased mitochondrial fission observed in TRPV4 KO microglia could contribute to the pathology of neurodegenerative diseases, where mitochondrial dysfunction and impaired microglial activity are common. Future research should focus on investigating the role of TRPV4 in microglial phagocytosis *in vitro* and *in vivo*, as well as exploring the effects of TRPV4 modulation on microglial function in disease models.

INTRODUCTION

Microglia are the resident immune cells of the central nervous system (CNS) and comprise 10-15% of all glial cells present in the brain (1-3). They are often referred to as the macrophages of the brain and have diverse functions, playing an important role in brain development and homeostasis, and CNS injury repair (2-4).

Unlike other cells of the CNS, microglia are derived from erythromyeloid progenitors (EMPs) that develop in the yolk sac during the embryonic phase (5). Subsets of these EMPs mature into C-X3-X Motif Chemokine Receptor 1 (CX3CR1) positive cells and become microglia progenitors. Microglia progenitors then migrate to the brain, and this continues until the blood-brain barrier (BBB) is fully formed (5, 6). After reaching their final location, the cells become quiescent (resting) and present a ramified morphology; microglia possess a small, round cell body with little cytoplasm and numerous branching processes (7). The microglia population is maintained by self-renewal, which is the only source of new microglia in the healthy brain (5). These ramified microglia possess a level of motility for surveillance and protection of the CNS. They constantly survey the surrounding environment by

process extension and retraction, enabling interaction with neurons, astrocytes and blood vessels either through direct contact or through secretion of mediators (3, 7-9). Because of this process extension, microglia can swiftly respond to damage or infections in the brain. When harmful molecules are present, microglia become activated and undergo morphological and functional transformations from a ramified state to an amoeboid state (9). Microglia now show an enlarged cell body with short, thick pseudopodia that enable them, aided by chemotactic cues, to move swiftly to the site of injury. During development, microglia contribute to the formation of the final neuronal network by stimulating vascularization and assisting in synaptic pruning. In the adult brain, they maintain homeostasis by synaptic remodeling and by removing proteins and debris that accumulate in the brain (6, 9). When the CNS is injured or in order to maintain brain homeostasis, microglia are responsible for phagocytosis of apoptotic cells, microbes, and aggregates that can compromise homeostasis (2, 8).

Molecular microglia identification

Microglial identification is based on the expression of specific genes that are enriched in microglia, commonly named microglia markers. Microglia markers include surface, intracellular and released molecules. There are many general microglia markers that can be detected irrespective of the cell phenotype. The most used markers are the cytoplasmic marker ionized calcium-binding adapter molecule 1 (IBA-1), cluster of differentiation receptors (CD68, CD11b, CD14, CD45, CD80 and CD115), fractalkine receptor CX3CR1, ferritin, F4/80 and vimentin (7). CX3CR1 is used to generate enhanced green fluorescent protein (eGFP) positive microglia. The most specific markers are the surface markers purinergic receptor P2Y12R and transmembrane protein 119 (TREM119) (7, 10).

Phagocytic process

When a cell goes into apoptosis, microglia will initiate phagocytosis to prevent further damage. The process of phagocytosis was first observed by Élie Metchnikoff and takes place in different phases: [1] the find-me phase, [2] the eat-me phase, and [3] the digest-me phase (Fig.1) (11).

Find-me

In the find-me phase, microglia will recognize exposed find-me signals released by the apoptotic cell, myelin debris or by excessive synapses (12). These signals can include nucleotide adenosine triphosphate (ATP) and uridine triphosphate (UTP), attracting microglia by activating the P2Y12 receptor (13, 14). One of the most important chemotactic signals is CX3C Ligand 1 (CX3CL1), better known as fractalkine, released by neurons or synapses, which attracts microglia via the CX3CR1 receptor (13, 15). The pro-inflammatory bacterial lipopolysaccharide (LPS) is also an important signal, which drives microglial activation through the toll-like receptor (TLR)-4 and nuclear factor kB (NF-kB) pathways (16).

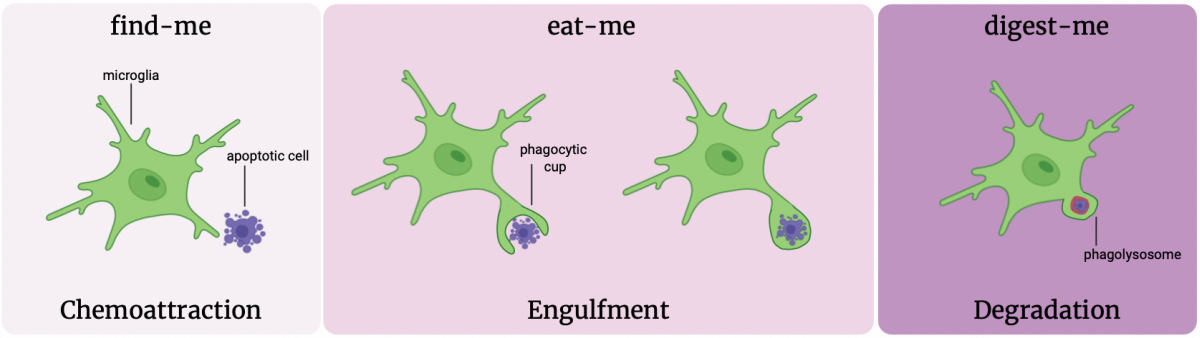

Figure 1: Three-step model of microglial phagocytosis. Activated microglia respond to chemoattractant molecules released by apoptotic cells, such as CX3CL1 and nucleotides such as ATP ('find-me" phase). Next, a connection is formed between the microglial receptor and a ligand in the membrane of the apoptotic cell, which leads to engulfment of the particle ("eat-me" phase). The phagolysosome will be fully degraded by the presence of an acidic pH and ROS formation ("digest-me" phase).
CX3CL1= C-X3-C Motif Chemokine Ligand 1, ATP= adenosine triphosphate, ROS= reactive oxygen species

Eat-me

Once microglia reach the target cell, contact is established through a receptor-ligand interaction to initiate the eat-me phase (17). The process of engulfment is the most important phase in phagocytosis. Microglia have several complementary membrane receptors that recognize the target to engulf them and distinguish them from living cells, which express do-not-eat-me signals such as CD47 (15, 17). A crucial eat-me signal is phosphatidylserine (PS), which is exposed on the cell surface of apoptotic cells (13, 18). To take up the particle, a phagocytic cup must be formed around the particle. This requires changes to the actin-myosin complex, which is formed by F-actin and non-muscle myosin II (19). Various pathways are involved in controlling the movement and localization of proteins and organelles within the cell. The most well-known receptors for intracellular signaling of phagocytosis are Fc receptors (FcR) and complement receptors (CRs) (figure 2).

Fc receptor signaling

Following recognition by FcR, FcR crosslinking and phosphorylation of immunoreceptor tyrosine-based activation motif (ITAM) on the cytoplasmic tail of FcR is induced by tyrosine kinases of the Src family (19, 20). This phosphorylation is responsible for the recruitment and phosphorylation of Spleen

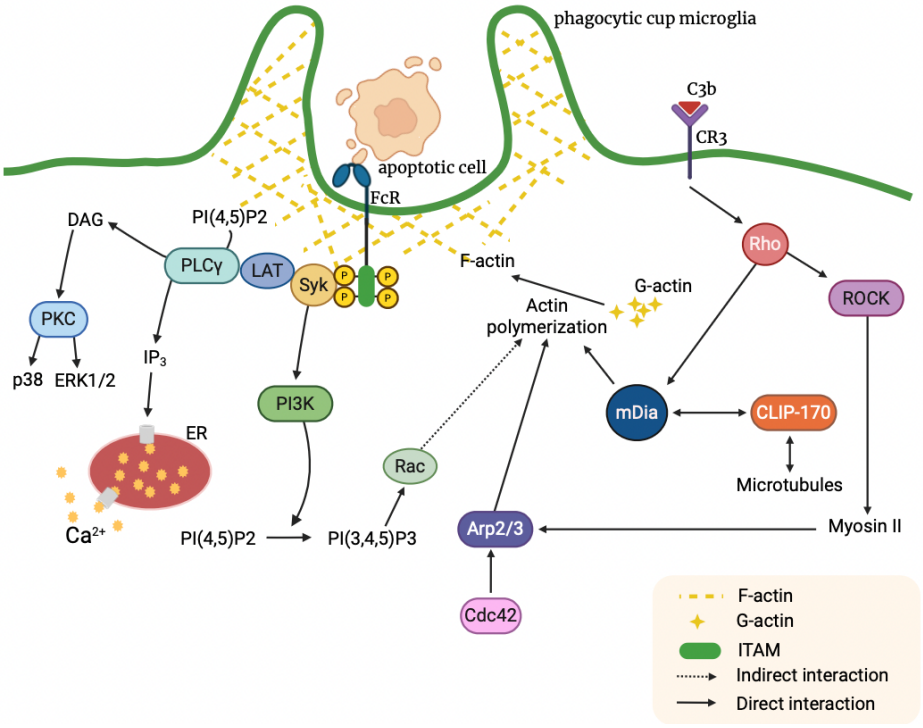

Figure 2: FcR-mediated and CR-mediated signaling for phagocytosis. **Left:** following recognition by FcR, FcR crosslinking and phosphorylation of ITAM on the cytoplasmic tail of FcR is induced by tyrosine kinases of the Src family. This phosphorylation is responsible for the recruitment and phosphotylation of Syk. Syk then triggers the conversion of PI(4,5)P2 to PI(3,4,5)P3 through PI3K. PI(3,4,5)P3 activates Rac, which contributes to actin polymerization together with cdc42. Phosphorylated Syk also generates DAG and IP3 from PI(4,5)P2. DAG induces PKC-mediated activation of p38 and ERK signaling. IP3 triggers Ca2+ release from the ER to the cytosol. **Right:** CR binds to a complement component and initiates the signaling cascade via Rho. Rho activated ROCK, which induces myosin II phosphorylation and recruits the Arp2/3 complex, leading to actin polymerization. Activated Rho also recruits mDia, which mediates actin polymerization. mDia also interacts with CLIP-170, which in turn interacts with microtubules to promote further actin polymerization.
FcR= Fc receptor, CR= complement receptor, ITAM= immunoreceptor tyrosine-based activation motif, LAT= linkerfor activation of T-cells, PI3K= phosphatidylinositol 3 kinase, PLCγ= phospholipase Cγ, DAG= diacylglycerol, IP3= inositol triphosphate, ER= endoplasmic reticulum, PKC= protein kinase C, ROCK= Rho-associated kinase, mDia= mammalian diaphanous-related formin-1.

tyrosine kinase (Syk). Syk then triggers the conversion of PI(4,5)P2 to PI(3,4,5)P3 through phosphatidylinositol 3 kinase (PI3K) (15, 21, 22). PI(3,4,5)P3 activates Rac, which contributes to actin polymerization together with Cdc42 (20, 22). Phosphorylated Syk also generates diacylglycerol (DAG) and inositol triphosphate (IP3) from PI(4,5)P2. DAG induces protein kinase C (PKC)-mediated activation of p38 and ERK signaling. IP3 triggers Ca^{2+} release from the ER to the cytosol(20, 22).

Complement receptor signaling

Complement-mediated phagocytosis is accomplished by recognition of bound complement components by their corresponding CRs (20, 23). Unlike FC-mediated phagocytosis, the actin and microtubule cytoskeleton are required to engulf particles during CR-mediated phagocytosis (20, 24). CR3 binds to a complement component C3b and initiates the signaling cascade via Rho, leading to F-actin polymerization. Rho activates ROCK, which induces myosin II phosphorylation and recruits the Arp2/3 complex, leading to actin assembly at the phagocytic cup (11, 20). Activated Rho also recruits mDia, which also mediates actin polymerization. mDia also interacts with CLIP-170, which interacts with microtubules to promote further actin polymerization (11).

Digest-me

Once the edges of the phagocytic cup reach the apex of the particle, they make contact and merge, leading to fission of the membrane to release the phagosome (25, 26). Ingestion of the target is then followed by maturation of the phagosome by interacting with other endocytic compartments, ending with fusion between the phagosome and the lysosome, forming a phagolysosome (12, 25, 27). The phagosome is transported to the lysosome by dynein-mediated movement of the phagosome along the microtubules (28). Microtubules serve as tracks for the transport of the phagosome to reach the lysosome positioned at the center of the cell to enable membrane fusion (28). Once the phagolysosome is formed, the engulfed particle is broken down. The phagolysosomal content is not only very acidic due to proton pumps such as vacuolar ATPases, but it also contains hydrolytic enzymes, proteases, and reactive oxygen species (ROS) to digest the target (11, 25). Eventually, the phagolysosome decreases in size, undergoes fragmentation and disappears (25).

The transient receptor potential vanilloid 4 channel

To maintain a healthy state in the brain and for microglia to properly perform their function, constant cell movement is required through process extension and migration (29). This requires cytoskeletal rearrangement, which is regulated at subcellular levels. Process motility and extension is mediated by Ca^{2+} (30). Because of this, microglia present a plethora of proteins that mediate the Ca^{2+} uptake and its trafficking. Local Ca^{2+} increase can be initiated by the transient receptor potential (TRP) channel family. The transient receptor potential vanilloid 4 (TRPV4) is a nonselective cation channel permeable for Ca^{2+} and plays a role in the regulation of microglial morphology. TRPV4 can be activated by moderate temperature changes, cell swelling and stretch, making it a thermo- and mechanosensitive channel (31). This channel is located on the membrane of microglia and has been identified along proteins that are part of the cytoskeleton, such as actin, making it an important player in Ca^{2+} homeostasis of microglia (32).

When phagocytosis of a particle occurs, actin polymerization will drive the rearrangement of the cytoskeleton and plasma membrane of the microglia to surround the phagocytic target, forming the phagocytic cup (33). Because of the stretching of the membrane, the TRPV4 channel becomes activated, and the intracellular Ca^{2+} concentration increases, contributing to cell movement (34). The closing of the phagocytic cup is thus heavily dependent on cytoskeletal reorganization. A lot of energy is required to facilitate this movement, which is provided by mitochondria.

Mitochondria and their function

Phagocytic cup formation is heavily dependent on cytoskeletal reorganization, and this requires energy to facilitate movement of the cell to take up a particle. This energy is delivered by mitochondria, maternally inherited organelles that produce most of the cell's energy in the form of ATP via oxidative phosphorylation (OXPHOS) (35-37). They consist of two distinct and functionally separate membranes: the outer membrane (OM) and the inner membrane (IM), which enclose the intermembrane

space and matrix compartments, respectively (29). Mitochondria also possess their own genome (mtDNA), which replicates independently of the nuclear genome (38). Beyond their role in energy production, they are also critical organelles for many other processes, such as production of ROS and cell survival (35, 39). Mitochondria are important Ca^{2+}storage sites and shape the distribution of Ca^{2+} by buffering Ca^{2+} flux from the plasma membrane and endoplasmic reticulum (ER), thus regulating intracellular calcium responses, one of the most omnipresent signaling second messengers employed in living cells (35, 38, 39). Mitochondria can perform multiple activities such as mitochondrial motility, fission and fusion, and tethering (35, 38). These activities decide the overall shape, connectedness, and location of mitochondria within cells (38).

Mitochondrial movement

Appropriate distribution of the mitochondrial network is essential for cell survival. Mitochondria form a dynamic network in the cell, responsible for energy production, Ca^{2+} homeostasis and cell signaling (40). In most cells, they form a branched tubular network that is distributed throughout the cell. This mitochondrial population can move in different directions along microtubule tracks; movement away from the nucleus is termed anterograde transport, while movement toward the nucleus is known as retrograde transport (Fig. 3) (40, 41). Mitochondrial movement depends on actin filaments and microtubules, primarily driven by molecular motors along cytoskeletal elements. They utilize microtubule motors, which include plus-end kinesin motors mediating anterograde movement, and minus-end dynein motors mediating retrograde movement. An example of a plus-end kinesin is kinesin-1, also known as KIF5, which is critical for mitochondrial transport. Additionally, two members of the kinesin-3 family are associated with mitochondria: KIF1Bα and Kinesin-Like protein 6 (KLP6) (41). These motor proteins are anchored to mitochondria by adaptor proteins. The best-known motor/adaptor complex of anterograde mitochondrial transport is the kinesin heavy chain

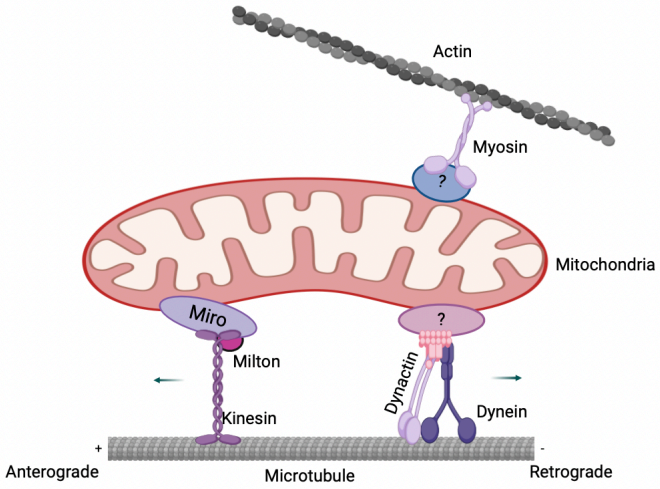

Figure 3: Mitochondria can move in different directions. Mitochondria can move along microtubule tracks and actin filaments through two mechanisms: anterograde and retrograde movement. **Anterograde movement:** the motor/adaptor complex KHC/Milton/Miro allows for anterograde movement away from the nucleus. Miro links the mitochondrial surface to Milton, which in turn binds to KHC that associated with microtubules. **Retrograde movement:** the dynein/dynactin complex allows retrograde movement towards the nucleus. Dynactin can bind to dynein and microtubules directly. Mitochondria can also be transported along **actin filaments**, where Myo19 was identified as a myosin motor the regulate actin-based mitochondrial transport.
KHC= kinesin heavy chain, Myo19= myosin 19

(KHC)/Milton/Miro complex (40, 41). Miro, a mitochondrial Rho GTPase, functions as a receptor that links the mitochondrial surface of the mitochondria to the microtubule motor protein kinesin Milton, which in turn binds to KHC (38, 41). This complex allows mitochondria to associate with microtubules and closely regulates mitochondrial movement. As for retrograde movement, the mechanisms are less clear. It has been shown that dynein is the motor for this type of transport and dynactin can bind to dynein and microtubules directly (41). Mitochondria can also be transported along actin filaments, but little is known of actin motors or their adaptors. Myo19 was identified as a myosin motor, exclusively localized to mitochondria regulating actin-based mitochondrial transport (41, 42).
Mitochondrial motility can be regulated by cytosolic Ca^{2+}. Resting levels of Ca^{2+} permit mitochondrial movement, while an increase in cytosolic calcium is coupled to an inhibition of mitochondrial motility in neurons (38, 40, 41). Miro can serve as a Ca^{2+} sensor that controls mitochondrial motility; Ca^{2+} binds to Miro in the motor/adaptor complex, interfering with the KHC motor/microtubule binding. This will lead to dissociation of the mitochondria from the microtubules, halting movement (41).

Mitochondrial fission and fusion
Being a vital cellular organelle, the maintenance of mitochondrial homeostasis is crucial (43). Mitochondria continuously undergo changes in their number and morphology through the process of fission and fusion. These processes are mediated by GTPases to remodel membranes in cells. Fission is the process where a mitochondrion divides itself into two mitochondria. This process plays different roles, such as proper distribution of mitochondria, cytochrome c release during apoptosis and most importantly, the removal of impaired mitochondria by mitophagy (43). In mitochondrial fusion, two mitochondria are joined at the OM and IM interfaces via three membrane GTPases, mitofusion 1 (MFN1), MFN2 and optic atrophy protein 1 (OPA1) (35, 43). Fusion is crucial as it allows the exchange of genes and metabolites between the fusing mitochondria to enhance their overall function.

Glial mitochondria in neurodegenerative diseases
Mitochondrial dysfunction can contribute to the development of many neurological diseases. A review by Zhou et al. (2018) discusses mitochondrial dysregulation in several neurological disorders, such as Alzheimer's disease (AD) and epilepsy (37). In AD, amyloid β (Aβ) deposition, a peptide that forms extracellular senile plaques, can damage mtDNA, alter mitochondrial metabolism, and change the mitochondrial membrane permeability, leading to microglial activation and neuroinflammation (37, 44). Further, microglia could release ROS and reactive nitrogen from damaged mitochondria that were not properly removed by mitophagy. This further damages the surrounding environment and amplifies the neuroinflammation, ultimately leading to AD (44).

To date, much of the work on mitochondrial properties in the CNS has focused on neuronal approaches (45, 46). However, the typical movement of mitochondria during microglial phagocytosis remains elusive. It is necessary to consider the importance of mitochondria in microglia, as these cells comprise a significant portion of cells in the CNS and perform essential functions in the development and function of the brain (36). Microglia play a significant role in various diseases such as multiple sclerosis, AD, and schizophrenia (37, 47). In such diseases, their motility plays an important role in the phagocytosis of harmful particles. Beeken et al. (2022) recently showed that after acute inhibition of microglial TRPV4 with the TRPV4 antagonist GSK21, cytoskeletal dynamics were decreased alongside a decrease in morphological complexity and brain surveillance (48). As TRPV4 is a Ca^{2+} channel, the inhibition of TRPV4 could have a possible effect on mitochondrial dynamics and microglial phagocytosis, offering an opportunity to study the molecular mechanisms underlying mitochondrial movement during phagocytosis. This project aims to determine the mitochondrial distribution in microglia and whether TRPV4 is present at the phagocytic cup. Additionally, the role of TRPV4 in mitochondrial dynamics and movement during microglial phagocytosis is investigated using TRPV4 WT and KO microglia and a TRPV4 antagonist. **We therefore hypothesize that TRPV4 and mitochondria are present at the phagocytic cup site, and that mitochondrial dynamics and movement in mouse microglia during phagocytosis will increase when TRPV4 is absent.**
By understanding the molecular mechanisms of mitochondrial movement in microglial phagocytosis,

valuable insights can be obtained into potential disease mechanisms associated with mitochondrial and microglial dysfunction, such as schizophrenia, where microglial function is altered.

EXPERIMENTAL PROCEDURES

Animals – All experiments were conducted using 21-day-old WT and TRPV4 KO C57BL/6J littermates (in-house breeding). All used experimental animals express eGFP under the CX3CR1 promotor. Animals were housed in the animal facility on a 12h light/dark cycle with free access to food and water. All experimental procedures were performed by following the EU Directive 2012/63/EU law for animal testing and were approved by the local ethical committee (Ethical Commission for Animal Experimentation, UHasselt, Diepenbeek, Belgium, ID 202033B).

Genotyping – The genotype of mice was confirmed by PCR. DNA was extracted from toe biopsies using the KAPA Hotstart Mouse Genotyping Kit (KAPA Biosystems inc., Wilmington, MA, USA). Extraction buffer was added to the DNA samples whereafter they were placed on a 75° C thermocycler for 10 minutes to lyse the cells and release the DNA, followed by 5 minutes at 95° C to activate the enzyme. The DNA sample was then 1:10 diluted in MilliQ. The sample was added to the Fast Genotyping PCR mix (Kapa Biosystems inc., Wilmington, MA, USA). The used primer sequences can be found in supplementary table 1. PCR for TRPV4 was performed for 36 cycles with: [1] 3 min of denaturation at 95°C, [2] primer annealing for 15s at 95° C, 15s at 60°C and 15s at 72° C for 35 cycles, and [3] 60s of elongation at 72° C. The DNA was held at 12° C and run on a 2% agarose gel for 1h30 minutes at 145V. PCR for CX3CR1 was performed for 36 cycles with: [1] 3 min of denaturation at 94° C, [2] primer annealing for 30s at 94° C, 30s at 64° C with an increment of -0.2° C and 1 min at 72° C for 35 cycles, and [3] 7 min of elongation at 72° C. The DNA was held at 4°C and run on a 3% agarose gel for 1h30 min at 145V.

Isolation of primary microglia – Primary microglia cultures were prepared from the brains of postnatal day (P) 21 C57BL/6J mice. Pups of both sexes were included in each culture. Mice were sacrificed by decapitation. Brains were then removed and dissected under a sterile ventilation hood in Hanks' Balanced Salt Solution (HBSS) to obtain the cortex. The tissue was mechanically dissociated in cold Dulbecco's Modified Eagle Medium (DMEM, Thermo Fisher Scientific, Waltham, MA, USA) supplemented with 1% penicillin/streptomycin (p/s, Sigma-Aldrich, Saint-Louis, MO, USA) using different sized pipets. 110 mg/ml of DNase and 16 units/mg protein of papain were added, followed by 30 minutes of incubation at 37°C for enzymatic cell dissociation. The sample was then filtered through a 70 µm strainer, washed with DMEM + 1% p/s and centrifuged to obtain the cell suspension. After centrifugation, cells were placed in a Percoll gradient to isolate the macrophages and remove the myelin and blood cells. The cell suspension was then centrifuged at 650 g for 25 min at room temperature (RT). The supernatant containing myelin was discarded and the cells were collected from the interphase between the 30% and 70% Percoll gradient, after which they were resuspended in PBS to aid the removal of the density gradient medium. After centrifugation at 500 g for 5 min at 4° C, the cells underwent Magnetic-Activated Cell Sorting (MACS) to select microglia. Briefly, the pellet was resuspended in cold MACS buffer (1x PBS supplemented with 0,05% FBS and 0,05% EDTA) and incubated with CD11b magnetic microbeads (Miltenyi Biotec, Bergisch Gladbach, Germany), a microglial marker, at 4° C for 15 min. The cell suspension was then run through an MS separation column (Miltenyi Biotech, Bergisch Gladbach, Germany) fitted into an OctoMACS cell separator (Miltenyi Biotech, Bergisch Gladbach, Germany). Unlabeled cells passed through the column while CD11b-labeled cells remained in the magnetic field of the MS column. After washing the column with MACS buffer, the column was removed from the OctoMACS separator and flushed with MACS buffer to collect the CD11b-positive cell suspension, later referred to as microglia. Microglia were then brought into culture to use in further experiments.

Culture of primary microglia – After MACS sorting, the microglia were seeded onto Poly-D-Lysine (PDL, 1:5 dilution in PBS 1x, A3890401, Thermo Fisher Scientific, Waltham, MA, USA) and collagen coated glass coverslips in a 24 well plate at a density of 200.000 cells per well or onto PDL

and collagen coated 2 well-inserts mounted on a MatTek dish at a density of 23.200 cells/well. Cells were maintained in 10:10:1 culture medium (DMEM supplemented with 10% Horse Serum, 10% Fetal Bovine Serum and 1% p/s) at 37°C in an incubator with 5% CO_2 for 7 days. After one week, the medium was changed to TIC medium (short for TGF-β, IL-34, and Cholesterol) consisting of DMEM F12 (M22426, Thermo Fisher Scientific, Waltham, MA, USA) supplemented with 5µg/ml Insulin, 5µg/ml N-acteyl-Cystein, 100 µg/ml Apo Transferrin, 1 µg/ml Heparan sulphate, 2 µg/ml Human TGF β, 100 ng/ml murine IL-34, 100 ng/ml Na+-Selenite, 1.5 µg/ml cholesterol, and 2 mM L-glutamine to induce microglial branching.

Induction of phagocytic cup – When RAW 264.7 cells reached 90% confluence, cells were detached using a cell scraper and centrifuged at 400g for 5 minutes. The pellet was then resuspended in Optimem (31985062, Thermo Fisher Scientific, Waltham, MA, USA) and 2% paraformaldehyde (PFA, prepared in-house) was added for 10 min at RT for apoptotic cell generation. After 10 min incubation, the apoptotic cells were centrifuged at 400g for 5 minutes and washed with PBS to remove PFA residue. Cells were centrifuged, supernatant was removed, and the cells were incubated with WGA-647 (W32466, Invitrogen, Waltham, MA, USA) prepared in Optimem (1:200) for 10 min at RT to stain the membrane. Cells were centrifuged and washed twice with PBS. After washing, the apoptotic cells were counted and resuspended in Optimem. Apoptotic cells were incubated with WT and KO microglia at a 1:1 ratio for 15 min to induce phagocytosis. After incubation, microglia were washed twice with PBS to remove excess apoptotic cells and fixated with 4% PFA for 15 min at 4°C.

Immunocytochemistry – After culturing and branching the cells, the medium was removed, and the cells were washed with PBS to remove all traces of serum. Cells were fixed with 4% PFA for 15 min. After fixation, cells were washed and incubated with blocking buffer (BB, 5% BSA in PBS) for 1h at RT. Primary antibodies were prepared in BB at the following dilutions: anti-hsp60 (HB7863, 1:2000, HelloBio, Dunshaughlin, Republic of Ireland) and anti-TRPV4 KO validated (ACC-034, 1:500, Alomone Labs, Jerusalem, Israel). Cells were then incubated with primary antibodies overnight at 4°C on an orbital shaker. Secondary antibodies were prepared in BB at the following dilutions: goat anti-mouse 1:1000 (A11019, Life Technologies, CA, USA), donkey anti-rabbit 1:1000 (A10042, Life Technologies, CA, USA). Cells were incubated with the secondary antibodies for 1h at RT on an orbital shaker. After incubation, nuclei were stained with DAPI for 15 minutes and washed. Coverslips were mounted on a microscope slide using Fluoromount G (00-4958-02, Thermo Fisher Scientific, Waltham, MA, USA). Images were acquired using Plan-ApoChromat 20x/0.8 NA air, and Plan-ApoChromat 63x/1.4 NA oil immersion objectives on the LSM900 confocal microscope (Zeiss Group, Oberkochen, Germany).

Mitochondria tracking – One week after TIC medium change, WT and KO microglia were incubated with MitoTracker prepared in DMEM F12 ($1:10^5$) for 20 min at 37°C and 5% CO_2. After incubation, cells were switched to Optimem. Images were acquired using a C-ApoChromat 63x/1.20 NA water immersion objective on the LSM880 confocal microscope (Zeiss Group, Oberkochen, Germany). During imaging, focus was put on the branches, and Z-stacks were chosen such as to encompass the thickness of the branch to investigate the movement of mitochondria in these structures. Images were acquired every 35s for 30 cycles. After baseline measurements, GSK2193874 (GSK21, 10 µM, Tocris Bioscience, Bristol, UK), a TRPV4 inhibitor, was added to investigate the effect on mitochondrial dynamics.

Mitochondrial analysis – Obtained images were processed in Fiji ImageJ. Z-stacks were used to create a maximum intensity projection of each channel. For mitochondrial distribution, a sholl analysis was performed. Briefly, a binary image was created of the red (mitochondria) and green (eGFP) channels. On the eGFP binary image, the center of the nucleus was selected as a reference point and concentric shells were drawn with a step size of 2 µm until the end of the cell was reached. The concentric shells were overlaid onto the binary image of the mitochondria, and the white pixel value was calculated for each shell. Each shell was subtracted from the previous shell to obtain the

number of pixels per ring band. To obtain the percentage of mitochondrial pixels per ring band, the following formula was used:

$$\frac{mitochondrial\ white\ pixels}{total\ white\ pixels}\ x\ 100$$

The complexity of the mitochondrial network was investigated using the Fiji plugin 'Mitochondrial Analyzer'. Z-stacks of the mitochondria channel were grayscaled and preprocessed using the plugin. 3D and 4D analysis was performed per cell, and several mitochondrial parameters were obtained (suppl. table 2).

Statistical analysis – For all statistical analyses, GraphPad Prism 10 (San Diego, California, USA) was used. Data was checked for outliers using the Grubb's test. Normality of the data was checked using the Shapiro-Wilk test. Normally distributed data were analyzed by a one-way ANOVA test followed by a Tukey's post-hoc test or by the student's t-test. If data were not normally distributed, a Kruskal-Wallis test followed by the Dunn's multiple comparisons test was performed, or the Mann-Whitney test was performed. When comparing phenotypes between WT and KO, a two-way ANOVA test followed by the Šídák's multiple comparisons test was performed. Data are shown as mean ± standard error of the mean (SEM). All values of $p \leq 0.05$ are considered statistically significant.

RESULTS

Mitochondria are located more distally from the nucleus in TRPV4 KO microglia compared to WT – Microglia are highly motile cells and need ATP to facilitate movement of their processes. This energy is primarily generated by mitochondria. More energy is needed at the dynamic structures of the cell, which suggests that mitochondria are distributed more densely in these areas. However, how these mitochondria are specifically distributed throughout microglia remains unknown. Additionally, it remains unknown whether there is a difference in mitochondrial distribution between microglial phenotypes. In accordance with their functional state, three distinct microglial phenotypes were chosen to investigate the mitochondrial distribution: (1) branched microglia, characterized by three or more branches, (2) bipolar microglia that have two branches on opposite ends of the cell body, and (3) microglia with a lamellipodium and one branch, or a trailing edge (LTE) (Fig. 4A). Microglial reactivity increases from branched to LTE, which is the least reactive. To investigate the mitochondrial distribution in microglia, an immunohistochemical staining was performed on WT and TRPV4 KO $eGFP^+$ microglia. A HSP60 staining was done to visualize mitochondria in the microglia, and nuclei were stained with DAPI. To assess mitochondrial distribution, a sholl analysis was performed in Fiji ImageJ (Fig. 4B-H). The center of the nucleus was chosen as a reference point. No significant difference was observed between the phenotypes within the WT and KO groups, respectively (Fig. 4D-E). In WT microglia, the branched and LTE phenotypes tend to have a higher mitochondrial pixel value closer to the nucleus compared to bipolar microglia (Fig. 4D). In TRPV4 KO microglia, branched cells showed a similar trend (Fig. 4E). Additionally, the difference in mitochondrial distribution between WT and TRPV4 KO microglia was assessed (Fig. 4F-H). No significant difference between WT and KO was observed in branched and bipolar microglia (Fig. 4F, 4H). In branched KO microglia, mitochondria tend to be slightly more dispersed compared to WT. Additionally, branched KO microglia exhibited longer branches compared to WT, although cell size did not differ significantly (Fig. 4C, Suppl. Fig 1A). WT and KO microglia had a significant difference in mitochondrial distribution for the LTE phenotype (Fig. 4G). WT LTE microglia show a significantly higher mitochondrial pixel value closer to the nucleus, while in the KO, mitochondria are distributed further throughout the cell. Taken together, these findings suggest a more widespread mitochondrial distribution in TRPV4 KO microglia compared to WT, particularly in LTE microglia.

TRPV4 KO microglia display a higher mitochondrial count and a larger surface area compared to WT – As previously mentioned, TRPV4 KO microglia display a more dispersed mitochondrial distribution compared to WT microglia. Since mitochondria serve as critical Ca^{2+} storage sites, the knockout of the TRPV4 channel could potentially affect mitochondrial dynamics, such as fission and fusion.

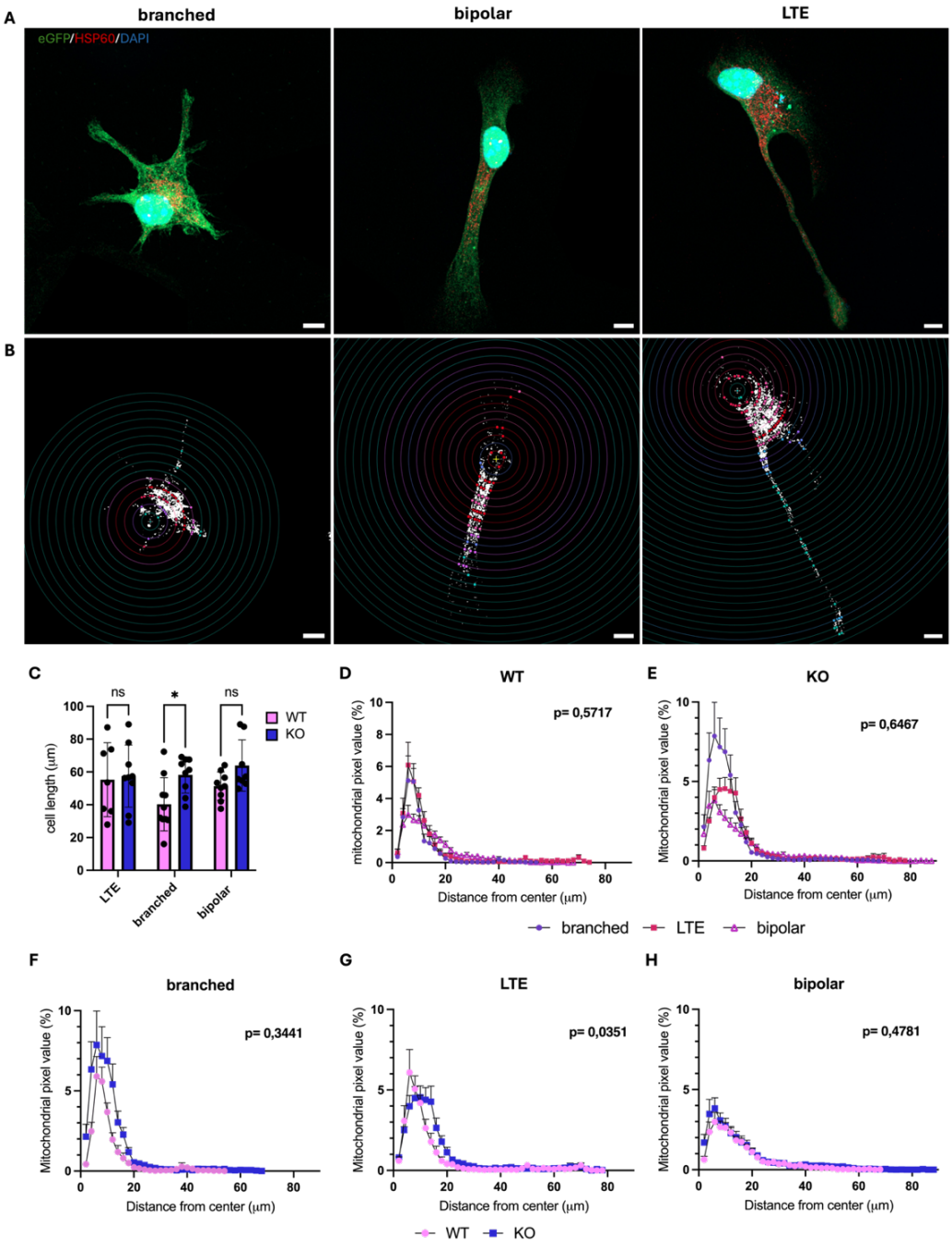

Figure 4: Mitochondrial distribution is equal between phenotypes in WT and KO microglia. **(A)** Representative immunohistochemical images of mitochondrial distribution (hsp60, red) in WT and KO microglia (eGFP, green). Nuclei were stained with DAPI (blue). Three distinct phenotypes were observed; branched, bipolar and lamellipodium with trailing edge (LTE). **(B)** Representative images of each phenotype for Sholl analysis. Concentric circles were drawn starting from the nuclei (reference point) until the end of the cell was reached. **(C-D)** Quantification of the difference in mitochondrial distribution between phenotypes for WT (n_B= 9, n_{LTE}= 7, n_{bip}= 9) **(C)** and KO microglia (n_B= 9, n_{LTE} = 9, n_{bip}= 8) **(D)**. **(E-G)** Quantification of the difference in mitochondrial distribution between WT and KO microglia for branched **(E)**, LTE **(F)**, and bipolar **(G)** microglia. Scalebar represents 5 µm. Statistical significance was assessed using the Kruskal-Wallis test (*p <0.05). Data represent mean ±SEM.
WT = wild-type, KO= knockout, eGFP= enhanced green fluorescent protein, B= branched, bip= bipolar

Additionally, it remains unclear whether different microglial phenotypes influence mitochondrial parameters. Accordingly, mitochondrial dynamics among branched, bipolar, and LTE phenotypes in WT and KO microglia were investigated using mitochondrial network analysis performed in Fiji ImageJ (Fig. 5A-C). Phenotypic differences in mitochondrial dynamics were assessed for both WT and KO microglia (Suppl. Fig. 2). Bipolar WT microglia exhibited a significantly higher number of mitochondria compared to branched microglia (Suppl. Fig. 5A). LTE WT microglia had a significantly larger mean surface area than bipolar microglia, suggesting a bigger cell size (Suppl. Fig 2H). No other significant differences in mitochondrial dynamics were observed between phenotypes in both WT and KO microglia.

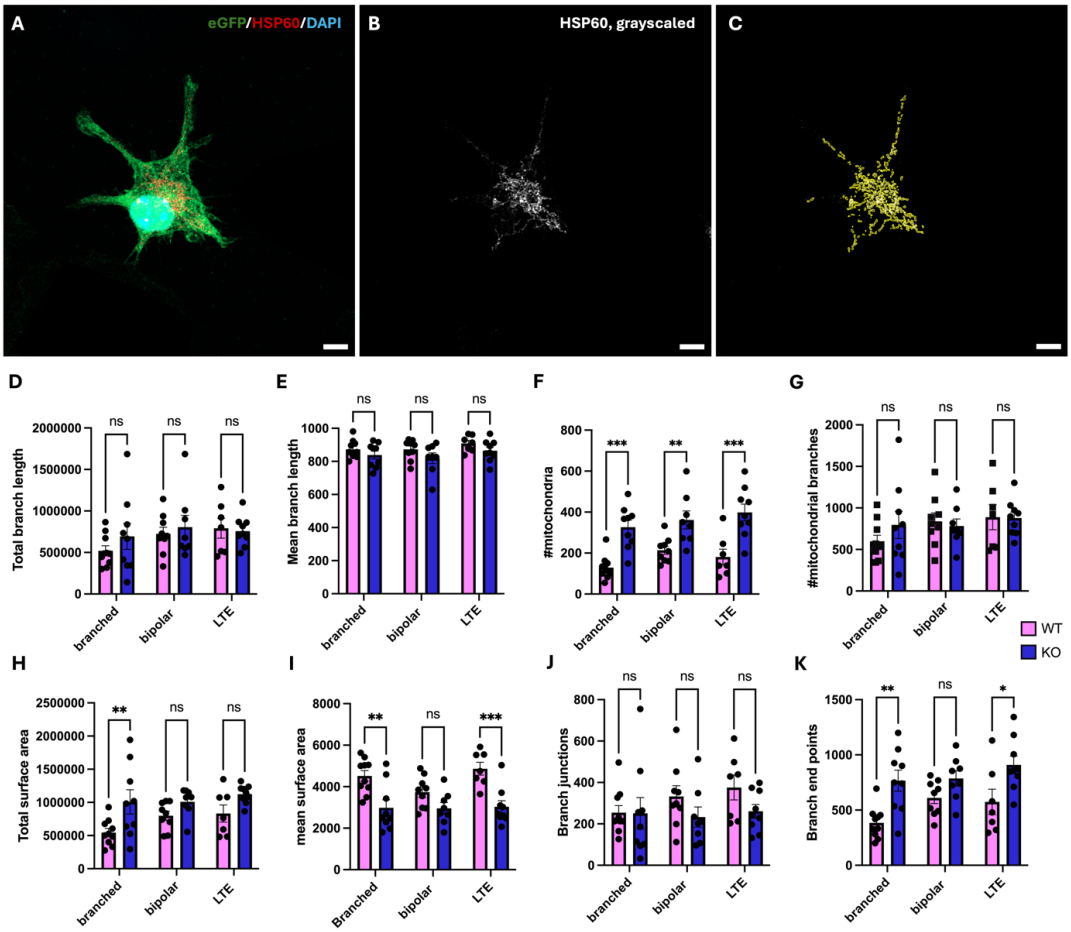

Figure 5: Mitochondrial analysis in WT and KO microglia. **(A)** Representative immunohistochemical image of mitochondria (hsp60, red) in WT and KO microglia (eGFP, green). Nuclei were stained with DAPI (blue). Three distinct phenotypes were observed; branched, bipolar and lamellipodium with trailing edge (LTE). **(B)** Representative image of mitochondria stained with hsp60, grayscaled. **(C)** representative image of the mitochondrial network analysis performed using Mitochondrial Analyzer in Fiji ImageJ. Mitochondria are outlined in yellow. **(D-I)** Quantification of the difference in total branch length **(D)**, mean branch length **(E)**, number of branches **(F)**, branch junctions **(G)**, branch end points **(H),** and number of mitochondria **(I)** between WT (n_B= 9, n_{LTE}= 7, n_{bip}= 9) and KO microglia (n_B= 9, n_{LTE} = 9, n_{bip}= 8) for each phenotype. Scalebar represents 5 µm. Statistical significance was assessed using a two-way anova mixed effects analysis. Normality was checked using the Shapiro-Wilk test (*p <0.05, **p<0,01, ***p<0,001). Data represent mean ±SEM.
WT = wild-type, KO= knockout, eGFP= enhanced green fluorescent protein, B= branched, bip= bipolar, ns= non-significant.

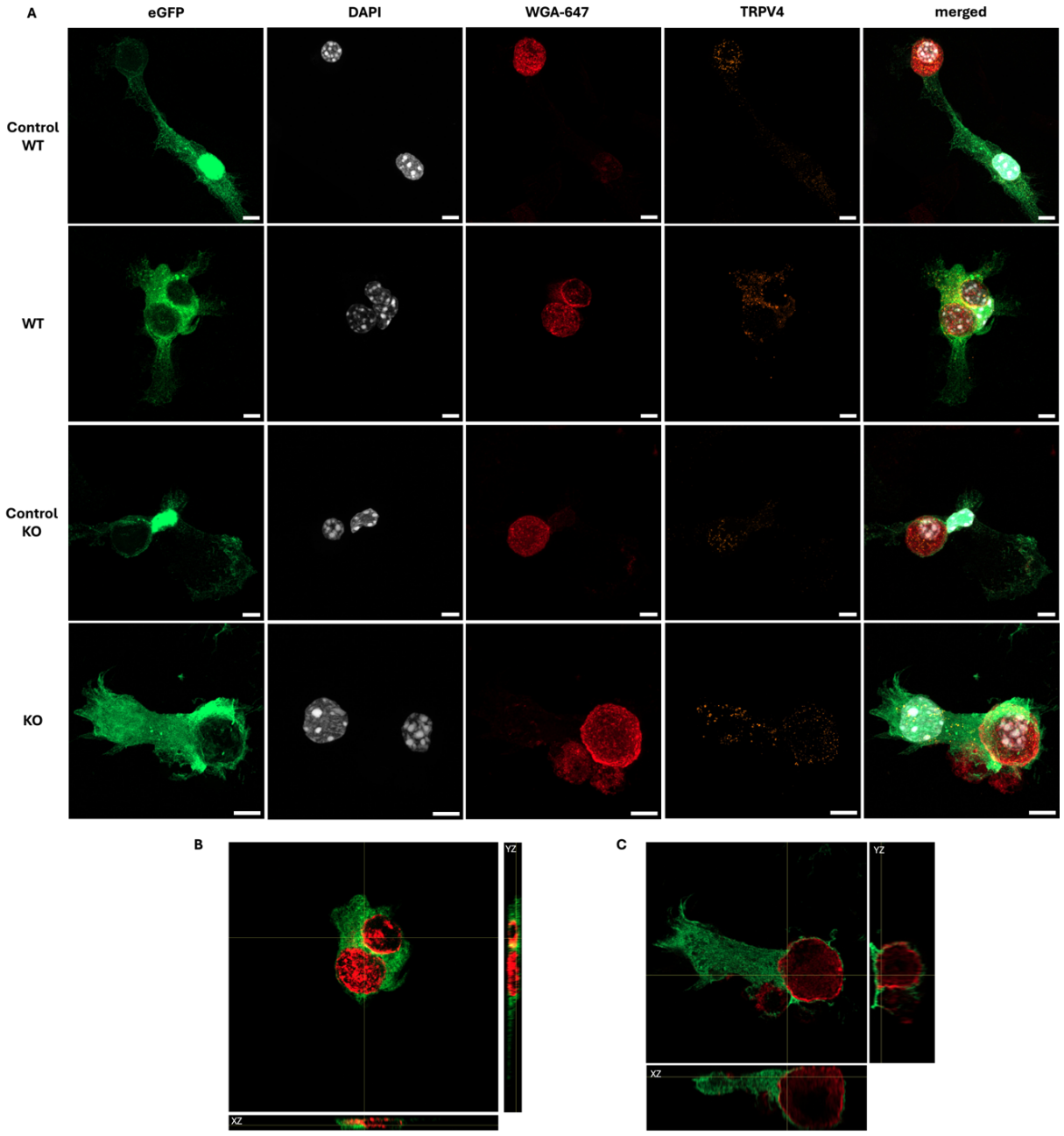

Figure 6: TRPV4 is present in the phagocytic cup of WT microglia. **(A)** Representative immunohistochemical images of TRPV4 (anti-TRPV4, orange) in WT and TRPV4 KO microglia (eGFP, green). Microglia were incubated with apoptotic RAW264.7 cells (WGA-647, red) for 15 min to induce phagocytic cup formation. Nuclei were stained with DAPI (blue). **(B-C)** orthogonal view of RAW264.7 cell and microglia indicates phagocytic cup formation in WT **(B)** and KO **(C)** microglia. Scalebar represents 5 µm.
WT = wild-type, TRPV4= transient receptor potential vanilloid 4, KO= knockout, eGFP= enhanced green fluorescent protein, WGA= wheat germ agglutin.

Various mitochondrial parameters were compared between WT and KO microglia (Fig. 5D-K). No significant differences were found in total branch length, mean branch length, number of mitochondrial branches, or branch junctions (Fig. 5D-E, 5G, 2J). However, KO branched microglia tended to have a higher total branch length and fewer mitochondrial branches compared to WT microglia of the same phenotype (Fig. 5D, 5G). In KO microglia, the number of mitochondrial branch junctions tended to be decreased in LTE and bipolar phenotypes (Fig. 5J). All KO phenotypes showed a significant increase in the total number of mitochondria (~300 per cell) compared to WT (~200 per cell). Branched KO microglia exhibited a higher total mitochondrial surface area, while their mean surface area was significantly decreased (Fig. 5H-I).

Additionally, branched and LTE KO microglia had significantly more branch endpoints compared to WT (Fig. 5K). These findings suggest that TRPV4 KO microglia have a significantly higher mitochondrial count and more branch endpoints.

TRPV4 is present at the phagocytic cup site of WT microglia – Phagocytosis is a highly dynamic process that requires energy to facilitate phagocytic cup formation. TRPV4 is a calcium channel present on the microglial membrane, which is activated by stretch of the membrane. To investigate whether TRPV4 influences microglial phagocytic cup formation and further on investigate whether blocking of TRPV4 influences mitochondrial dynamics, it first must be validated if TRPV4 is present at the phagocytic cup site. Immunohistochemical staining of TRPV4 in WT and TRPV4 KO eGFP^{+} microglia have shown a clear signal of TRPV4 in WT microglia surrounding apoptotic cells (Fig. 6A). Unexpectedly, TRPV4 expression was also detected in TRPV4 KO cells, where no expression should be present. Control images indicated that the TRPV4 signal was localized within the apoptotic RAW264.7 cells and not in the microglia (Fig. 6A). To ensure that microglia effectively engulf apoptotic cells, orthogonal views were reconstructed (Fig. 6B-C). Both WT and KO microglia exhibited cytosolic eGFP signal underneath and around the apoptotic cells, indicating phagocytic cup for-

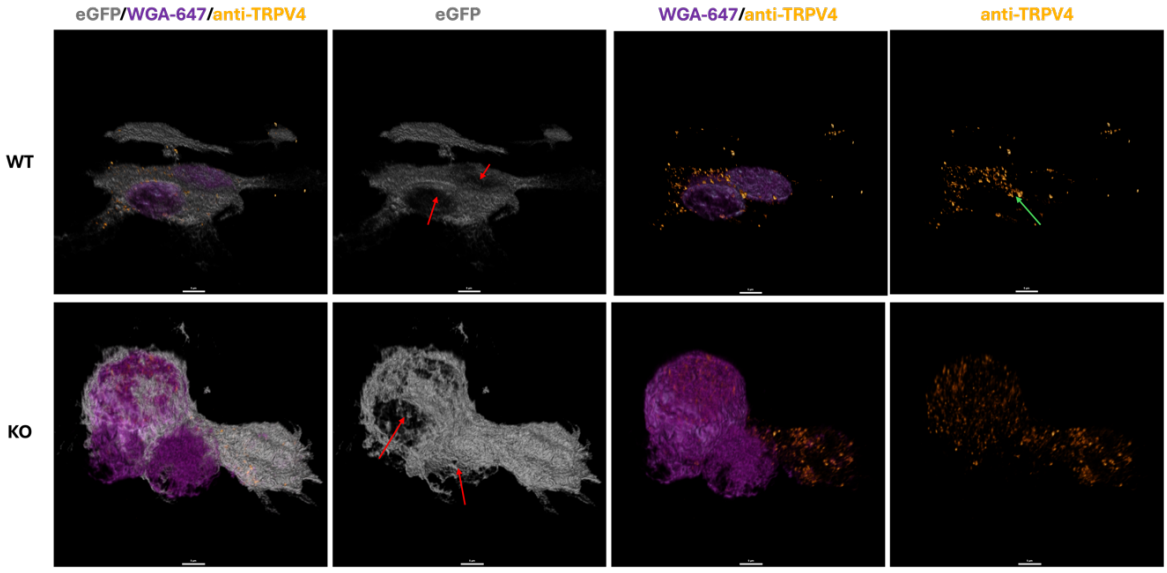

Figure 7: TRPV4 is present in the phagocytic cup of WT microglia. Representative 3D images of TRPV4 (anti-TRPV4, orange) in WT and TRPV4 KO microglia (eGFP, gray). Microglia were incubated with apoptotic RAW264.7 cells (WGA-647, purple) for 15 min to induce phagocytic cup formation (red arrow). TRPV4 is present in the phagocytic cup of WT microglia (green arrow). Scalebar represents 5 µm.
WT = wild-type, TRPV4= transient receptor potential vanilloid 4, KO= knockout, eGFP= enhanced green fluorescent protein, WGA= wheat germ agglutin.

mation. Further validation of phagocytic cup formation was achieved using 3D reconstruction (Fig. 7). The reconstruction revealed a layer of eGFP signal around apoptotic cells, highlighted by red arrows. In WT microglia, a distinct TRPV4 signal was observed between apoptotic cells, indicating TRPV4 presence at the phagocytic cup (green arrow). In KO microglia, although TRPV4 was detected in KO microglia, it was not localized at the phagocytic cup. These findings confirm the formation of clear phagocytic cups in microglia and demonstrate that TRPV4 is present at the phagocytic cup site in WT microglia.

Mitochondrial dynamics increase after acute TRPV4 inhibition – Having established that mitochondrial dynamics differ between WT and TRPV4 KO microglia, it was essential to examine how mitochondria behave upon acute TRPV4 inhibition and if this affects their dynamics (Fig. 8A). Live cell imaging after GSK21 addition has revealed a significant increase in all mitochondrial parameters (Fig. 8B-F). The higher mitochondrial count and increased surface area suggest enhanced mitochondrial fission (Fig. 8C, F). These results indicate that mitochondrial dynamics are significantly influenced by TRPV4 modulation, with acute TRPV4 inhibition leading to increased mitochondrial fission.

DISCUSSION

In this research, the aim was to investigate whether mitochondrial dynamics and movement in microglia increase when TRPV4 is absent. TRPV4 is a mechano-thermosensor permeable for Ca^{2+} important in microglial morphology. Despite the importance of TRPV4, its role in mitochondrial dynamics and movement in microglia remains to be elucidated. Using immunohistochemical staining and live-cell imaging techniques *in vitro*, we confirm that TRPV4 activity regulates mitochondrial dynamics in primary microglia. In homeostatic microglia, mitochondrial parameters, such as number of mitochondria and total mitochondrial surface area, significantly increase in TRPV4 KO microglia compared to WT microglia. More importantly, we demonstrate that acute inhibition of TRPV4 directly affects mitochondrial dynamics in WT microglia.

Appropriate distribution of the mitochondrial network is essential for cell survival. TRPV4 activity is known to regulate microglial morphology and migration, but how it affects mitochondrial distribution and its dynamics remains unknown (48). To get insights into the mitochondrial distribution, we analyzed the mitochondrial network obtained from immunohistochemical staining in WT and TRPV4 KO primary microglia using a sholl analysis. Knockout of TRPV4 caused a more widespread distribution of mitochondria from the nucleus compared to WT, particularly in LTE microglia. This suggests a shift in energy requirements. Wang et al. (2009) described the mechanism of Ca^{2+}-dependent regulation of mitochondrial motility in neurons (49). This study found that in neurons, Ca^{2+} binding permits Miro to directly interact with KHC, preventing interactions between the motor and microtubules, stopping mitochondrial movement. Consequently, when ATP is low, Ca^{2+} transport mechanisms are compromised, leading to an increase in cytosolic Ca^{2+}. Mitochondria will stop at these locations and are thus recruited to regions with low ATP to generate energy until normal levels are restored. This led the researchers to believe that this mechanism assists in balancing the distribution of mitochondria throughout the cell. With this knowledge, our findings can be interpreted; mitochondria are halted less because of lower Ca^{2+} levels, enabling further movement throughout the cell. Additionally, Goswami et al. (2010) discovered that TRPV4 modulates the microtubule stability in CHO-K1 cells. The microtubule cytoskeleton provided an anterograde force, while the actin cytoskeleton provides retrograde movement, determining the net movement of neurites (50). As TRPV4 is closely linked to actin, TRPV4 knockout could lead to disruption of the actin cytoskeleton, and thus partly retrograde movement. These findings are in line with our observations, as we see a more dispersed distribution of mitochondria away from the nucleus (anterograde) in TRPV4 KO microglia. It is worth noting that the mitochondrial distribution in microglia and neurons can differ. In terms of the intracellular localization of mitochondria, microglia have been found to have a higher proportion of mitochondria in the perinuclear region compared to neurons. This is thought to be related to the microglial role in monitoring the brain parenchyma and responding to changes in neuronal activity (51).

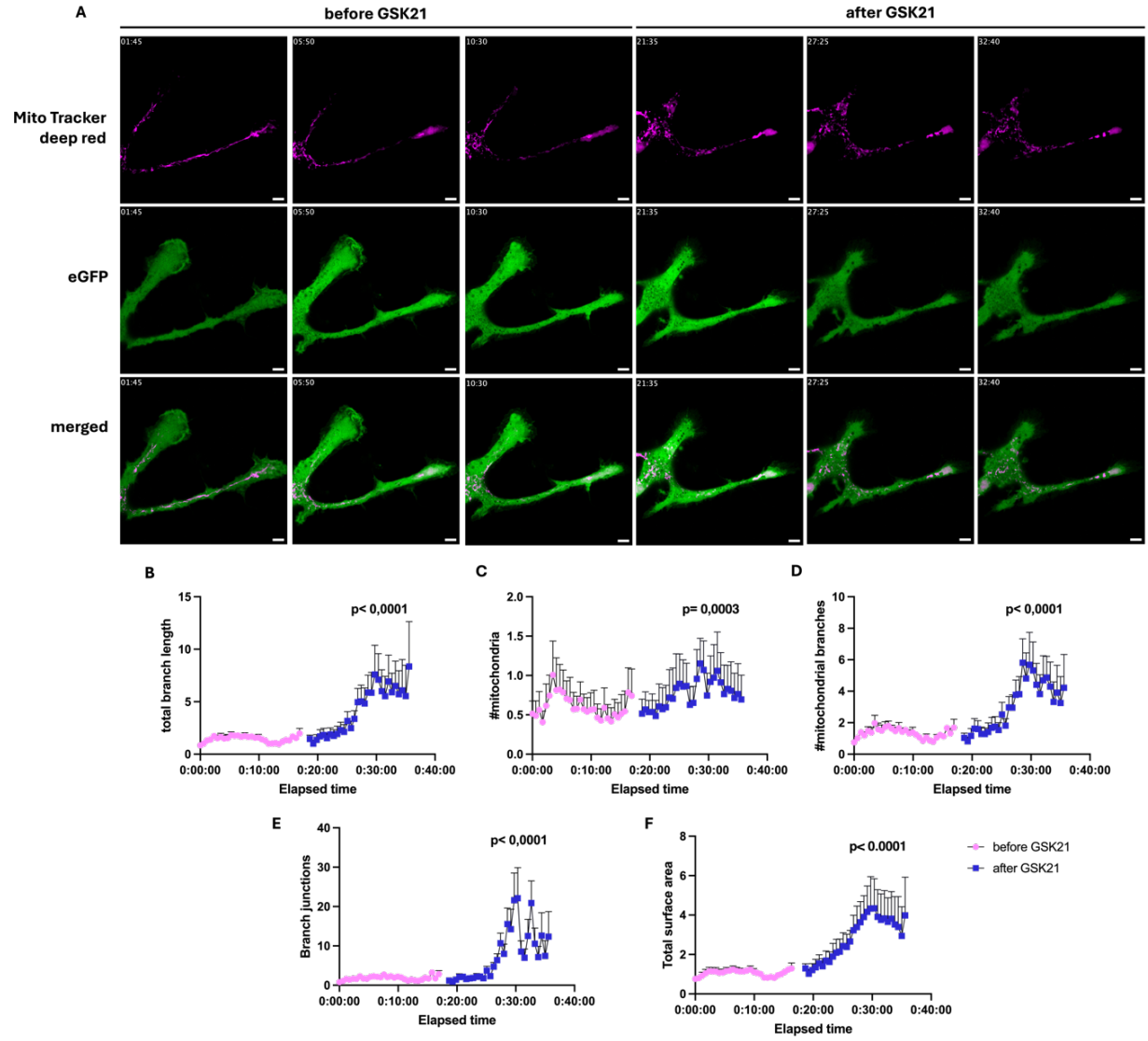

Figure 5: Mitochondrial analysis before and after administration of GSK21. **(A)** Representative immunohistochemical images of mitochondria (Mito Tracker deep red) in WT microglia (eGFP, green) before and after administration of the TRPV4 antagonist GSK21. **(B-E)** Quantification of mitochondrial parameters; difference in total branch length **(B)**, number of branches **(C)**, branch junctions **(D)**, and number of mitochondria **(E)** (n = 3). Scalebar represents 5 µm. Statistical significance was assessed using the Mann-Whitney test *p <0.05, **p<0,01, ***p<0,001, ****p<0,0001). Data represent mean ±SEM.
WT = wild-type, eGFP= enhanced green fluorescent protein, TRPV4= transient receptor potential vanilloid 4

Furthermore, these results led us to believe that TRPV4 influences not only the mitochondrial distribution, but their dynamics as well. Accordingly, several mitochondrial dynamic parameters were investigated using a mitochondrial network analysis performed in Fiji ImageJ. A brief overview of the results of the mitochondrial network analysis can be found in table 1. Our research suggests that TRPV4 KO microglia have a significantly higher mitochondrial count, more branch endpoints, and a bigger total surface area, indicative of more and smaller mitochondria in TRPV4 KO microglia. The number of

branch junctions was not significantly different between WT and KO. This parameter is critical for maintaining the structural integrity and functional efficiency of the mitochondrial network. More branch junctions suggest a higher degree of mitochondrial fusion, contributing to a more complex network (52). Taken together, these results point to increased mitochondrial fission in TRPV4 KO microglia. Mitochondrial fission and fusion are important processes that simultaneously and continuously occur, and these processes create a balance that regulates the overall morphology of the mitochondria (53, 54). During mitochondrial fusion, two or more organelles will fuse together to exchange mitochondrial material. Mitochondrial fission will divide a single organelle into two or more independent structures to allow redistribution of mitochondria or facilitation of segregation of damaged mitochondria (53, 54). As we observe a higher number of mitochondria in TRPV4 KO microglia together with a smaller mean surface area, we can conclude that fission allows for the formation of smaller mitochondria that efficiently redistribute throughout the cell to more energy demanding regions. A recent study by Acharya et al. (2022) found that TRPV4 interacts with MFN1/MFN2, two important dynamin-related GTPases in mitochondrial fusion (55). Upon TRPV4 activation in CHO-K1-V4 cells, mitochondria fuse together, and form aggregated mitochondria (55). These findings are in line with our results. TRPV4 was inactivated in primary microglia, thus likely leading to impaired fusion as the interaction between MFN1/MFN2 and TRPV4 is disrupted. This creates an imbalance between mitochondrial fission and fusion, which likely results in fragmented mitochondria because of higher fission. Fission will occur during cellular dysfunction and allows for redistribution of mitochondria throughout the cell. It could be that due to the absence of TRPV4, fission is increased to be able to handle mitophagy of damaged mitochondria. Mitophagy is better known as the removal of damaged mitochondria through autophagy (56).

An important function of microglia is phagocytosis, which requires a lot of energy provided by the mitochondria. TRPV4 is a mechanosensitive ion channel, which is activated upon stretching of the membrane during phagocytic cup formation. When TRPV4 becomes activated, there is an influx of Ca^{2+}. As mitochondria are important Ca^{2+} storage sites, we were interested to see if there is a correlation between the formation of the phagocytic cup, TRPV4 and mitochondrial distribution. We first confirmed that the eGFP signal seen in Fig. 3 originated from microglia, as minimal autofluorescence was detected in apoptotic RAW264.7 cells, proving the formation of a microglial phagocytic cup (Suppl. Fig. 3). Secondly, we had to validate that TRPV4 was actually present in the phagocytic cup. Using immunohistochemical staining and 3D rendering of the phagocytic cup, we prove that TRPV4 is present on the membrane in the inner leaflet of the phagocytic cup of WT primary microglia.

Even though these results are promising, several factors must be considered. Firstly, TRPV4 signal is still visible in RAW264.7 cells in the respective control images for WT and KO, even though only the secondary antibody is present. No signal was detected in the microglia itself, which led us to

Table 1: Summary of the main findings of the mitochondrial network analysis in WT and KO TRPV4 microglia. Three microglial phenotypes were investigated: (1) branched microglia with three or more branches, (2) bipolar microglia, with two branches opposite of each other, and (3) microglia with a lamellipodium and one branch, or a trailing edge (LTE). Table shows the results of the KO phenotypes compared to WT.

TRPV4 KO vs WT	Total branch length	Mean branch length	#mitochondria	#branches	Total surface area	Mean surface area	Branch junctions	Branch end points
Branched	ns	ns	↑	ns	↑	↓	ns	↑
Bipolar	ns	ns	↑	ns	ns	ns	ns	ns
LTE	ns	ns	↑	ns	ns	↓	ns	↑

WT= wild-type, KO= knockout, TRPV4= transient receptor potential vanilloid 4, ns= non-significant

believe that there is aspecific binding of the secondary antibody in RAW264.7 cells. As no aspecific binding is visible in the microglia itself, we can conclude that the TRPV4 signal present in the WT images is indeed TRPV4 present in the phagocytic cup.

Secondly, TRPV4 signal is detected in the images of the TRPV4 KO microglia. This could be due to aspecific binding of the antibody, but it seems unlikely as no TRPV4 signal was detected in control images of KO microglia. The apoptotic cells that were used in these experiments are RAW264.7 cells, macrophages with a lower expression of TRPV4 (57). It could be that in these images, the microglia already started breaking down the apoptotic cells and started taking up parts of the membrane, where TRPV4 is located. This motivates why TRPV4 signal is detected inside the microglia and not inside the lower RAW264.7 cell. A recent study by Holloman et al. (2023) proved that loss of TRPV4 increases microglial phagocytosis in vitro (58). As TRPV4 KO microglia show faster uptake of apoptotic cells, it is logical that at the same incubation times, KO microglia already show degradation of the apoptotic cells, while this is not yet visible in WT microglia at 15 min incubation. Taking these factors into account, these experiments should be repeated to better validate the presence of TRPV4 in the phagocytic cup. As RAW264.7 cells have TRPV4 expression, even though its expression is lower, it is difficult to determine if the TRPV4 signal present in the phagocytic cup is from the microglia or from the apoptotic cell (57). Consequently, a cell type that does not express TRPV4 should be used. According to Jin et al. (2011) RT-PCR and Western blot did not detect TRPV4 in WT HeLa cells, making this cell type a good candidate for apoptotic cell generation to use in further experiments (59). Additionally, more research must be performed to ensure there is no aspecific binding of the secondary antibody to the apoptotic cell.

Current research has mostly focused on how mitochondria move using microtubule tracks. It is known that mitochondria can also be transported along actin filaments. During phagocytic cup formation, actin becomes polymerized to facilitate phagocytic cup formation (11). As phagocytosis requires a lot of energy, it would be interesting to investigate whether mitochondrial distribution differs during phagocytosis and if mitochondria localize towards the phagocytic cup. Due to technical issues related to the microglial cultures, we were not able to include experiments of mitochondrial distribution and dynamics in phagocytic microglia during this study. These experiments should be performed to investigate possible differences in distribution between homeostatic and reactive microglia, and if there is a difference between TRPV4 WT and KO phagocytic microglia. Additionally, little is known of actin motor proteins and their adaptors. TRPV4 can directly interact with tubulin and actin, and TRPV4 inhibition leads to a decrease of actin-rich filopodia and tubulin dynamics (48). During phagocytosis, the Arp2/3 complex is recruited, which leads to actin assembly at the phagocytic cup together with mDia (11). As mitochondria can use actin for their movement, we expect mitochondria to be present in the phagocytic cup of microglia.

Lastly, we investigated mitochondrial dynamics in homeostatic WT microglia upon acute inhibition of TRPV4 with GSK21. Here, we prove that acute inhibition of TRPV4 directly affects mitochondrial dynamics in WT microglia. A significant increase in all investigated mitochondrial parameters was found after addition of GSK21, indicative of higher mitochondrial fission. When TRPV4 is inhibited, less Ca^{2+} is taken up in the cell, which could lead to cellular dysfunction. Several studies investigated mitochondrial movement in neurons, and found that resting levels of Ca^{2+} allow mitochondrial movement, while elevated Ca^{2+} levels inhibit mitochondrial motility in neurons (49, 60). A study by Wang et al. (2009) found that in neurons, Ca^{2+}-binding permits Miro to directly interact with the motor domain of kinesin 1, preventing interactions between the motor and microtubules. The best-known motor/adaptor complex of anterograde mitochondrial transport is the KHC/Milton/Miro complex (40, 41). Under normal conditions, KHC is recruited to mitochondria by the interaction of its C-terminal tail to the motor protein milton, which in turn binds to the mitochondrial surface by interacting with Miro, a mitochondrial Rho GTPase on the OM. In this confirmation, the N-terminal motor domain of KHC remains free to bind to microtubules to accomplish anterograde movement. However, in neuronal synapses, there is a high energy demand to maintain action potential firing. This is accompanied by a high Ca^{2+} influx at the synapse. Elevated

Ca^{2+} concentrations cause the KHC to lose its association with microtubules. KHC is thus switched to an inactive state where it directly binds to Miro and prevents interactions with microtubules, dissociating the mitochondria from the microtubules and halting the movement (41, 49). This mechanism in neurons could be alike in microglia. We have now demonstrated that there is a significantly higher number of mitochondria when less cytosolic Ca^{2+} is present due to blocking of the TRPV4 channel, which is in line with the findings in neurons (40, 41, 49). In this experiment, GSK21 was dissolved in MilliQ to obtain the correct concentration. To ensure our results are not due to the addition of MilliQ, this compound was used as a vehicle control (Suppl. Fig. 4). After addition of MilliQ, a significant decrease of all investigated mitochondrial parameters was visible (Suppl. Fig. 4A-E). This indicates that the significant increase in mitochondrial parameters is effectively due to the addition of GSK21. For the analysis, data was normalized by dividing the mitochondrial parameters by the vehicle control. Another method of analysis was performed to investigate how to effectively normalize the data (Suppl. Fig. 5). For this analysis, we first divided all values by the last datapoint obtained before adding GSK21 to normalize the data. The same was done for the vehicle control by dividing by the last datapoint obtained before adding MilliQ. The normalized values for GSK21 were then divided by the normalized values of the vehicle control (Suppl. Fig. 5A-E). With this method of analysis, error bars are higher, leading us to believe that the first method of analysis is more reliable. Due to technical issues related to the microglial cultures, we were not able to include the influence of TRPV4 inhibition in TRPV4 KO microglia. As TRPV4 is fully knocked out in these microglia, no significant effect would be expected when GSK21 is added. Additionally, we wanted to investigate differences in mitochondrial motility, speed, and fission/fusion rates when TRPV4 was blocked using MitoMeter. MitoMeter is a MATlab based application created by Lefebvre et al. (2022) to track mitochondria in live-cell time-lapse images (61). However, the application is still being optimized to use for our specific application. Further optimization of the MitoMeter application is necessary to extensively investigate the effect of GSK21 on the dynamics of mitochondria. Furthermore, conducting mitochondrial tracking in brain slices would provide valuable insights into *in situ* processes, which can be compared to the observations made in cell culture. A challenge in this type of experiment would be that a dense network of cells will have stained mitochondria. However, this can be circumvented by using animals with microglia specific labeled mitochondria (31). Interestingly, Chakraborty et al. (2023) showed formation of homotypic tunneling nanotubes (TNTs) between microglia, and heterotypic TNTs between microglia and neurons (62). These TNTs are functional and allow the movement of mitochondria from a healthy cell to a burdened cell, exerting a protective function. It is worth investigating whether microglia show a higher transfer of mitochondria and other cargo to other microglia and neurons, respectively, in the presence of GSK21. Additionally, it would be interesting to investigate the cytosolic Ca^{2+} levels using ratiometric time-lapse Ca^{2+} imaging to further strengthen that Ca^{2+} decreases while mitochondrial dynamics increase (31). It would be beneficial to also investigate the effect of acute inhibition of TRPV4 on microglial phagocytosis, and whether this affects phagocytic cup formation and mitochondrial dynamics around the phagocytic cup. Lastly, it would be interesting to repeat these experiments using a TRPV4 agonist to investigate the effect of acute TRPV4 activation on mitochondrial dynamics and phagocytosis.

Growing evidence has demonstrated a close association between mitochondrial dysfunction and microglia-driven neuroinflammation (44, 63, 64). In AD, accumulation of neurotoxic Aβ species can damage mitochondrial DNA, triggering mitochondrial dysfunction. A range of mitochondrial dysfunctions in microglia are already identified, including overproduction of mitochondrial ROS, elevated mitochondrial fragmentation, and reduced ATP levels, resulting in defective mitophagy (51, 65). When these mitochondria are not properly removed by mitophagy, it could lead to the activation of microglia that release harmful mitochondrial content into the extracellular environment (66). This in turn damages surrounding cells, which amplifies the inflammatory response, worsening disease progression. By further investigating the role of TRPV4 in mitochondrial dynamics, potential new therapeutic targets can be revealed. As GSK21 induces fission of mitochondria in our study, it

could enhance mitophagy of damaged mitochondria, and potentially reduce microglia-driven neuroinflammation in patients with AD.

CONCLUSION

To summarize, our study highlights the role of TRPV4 in regulating mitochondrial dynamics and distribution in mouse primary microglia. The increased mitochondrial fission observed in TRPV4 KO microglia could contribute to the pathology of neurodegenerative diseases, where mitochondrial dysfunction and impaired microglial activity are common. Future research should focus on investigating the role of TRPV4 in microglial phagocytosis *in vitro* and *in vivo*, as well as exploring the effects of TRPV4 modulation on microglial function in disease models. Additionally, studies using advanced imaging techniques to track mitochondrial movement in real-time during phagocytosis could provide deeper insights.

REFERENCES

1. Borst K, Dumas AA, Prinz M. Microglia: Immune and non-immune functions. Immunity. 2021;54(10):2194-208.
2. Colonna M, Butovsky O. Microglia Function in the Central Nervous System During Health and Neurodegeneration. Annu Rev Immunol. 2017;35:441-68.
3. Nayak D, Roth TL, McGavern DB. Microglia development and function. Annu Rev Immunol. 2014;32:367-402.
4. Wolf SA, Boddeke HW, Kettenmann H. Microglia in Physiology and Disease. Annu Rev Physiol. 2017;79:619-43.
5. Matcovitch-Natan O, Winter DR, Giladi A, Vargas Aguilar S, Spinrad A, Sarrazin S, et al. Microglia development follows a stepwise program to regulate brain homeostasis. Science. 2016;353(6301):aad8670.
6. Harry GJ. Microglia during development and aging. Pharmacol Ther. 2013;139(3):313-26.
7. Jurga AM, Paleczna M, Kuter KZ. Overview of General and Discriminating Markers of Differential Microglia Phenotypes. Front Cell Neurosci. 2020;14:198.
8. Zhang L, Cao Y, Zhang X, Gu X, Mao Y, Peng B. The origin and repopulation of microglia. Dev Neurobiol. 2022;82(1):112-24.
9. Wendimu MY, Hooks SB. Microglia Phenotypes in Aging and Neurodegenerative Diseases. Cells. 2022;11(13).
10. Paolicelli RC, Sierra A, Stevens B, Tremblay ME, Aguzzi A, Ajami B, et al. Microglia states and nomenclature: A field at its crossroads. Neuron. 2022;110(21):3458-83.
11. Rosales C, Uribe-Querol E. Phagocytosis: A Fundamental Process in Immunity. Biomed Res Int. 2017;2017:9042851.
12. Podlesny-Drabiniok A, Marcora E, Goate AM. Microglial Phagocytosis: A Disease-Associated Process Emerging from Alzheimer's Disease Genetics. Trends Neurosci. 2020;43(12):965-79.
13. Butler CA, Popescu AS, Kitchener EJA, Allendorf DH, Puigdellivol M, Brown GC. Microglial phagocytosis of neurons in neurodegeneration, and its regulation. J Neurochem. 2021;158(3):621-39.
14. Medina CB, Ravichandran KS. Do not let death do us part: 'find-me' signals in communication between dying cells and the phagocytes. Cell Death Differ. 2016;23(6):979-89.
15. Sierra A, Abiega O, Shahraz A, Neumann H. Janus-faced microglia: beneficial and detrimental consequences of microglial phagocytosis. Front Cell Neurosci. 2013;7:6.
16. Blank M, Enzlein T, Hopf C. LPS-induced lipid alterations in microglia revealed by MALDI mass spectrometry-based cell fingerprinting in neuroinflammation studies. Sci Rep. 2022;12(1):2908.
17. Janda E, Boi L, Carta AR. Microglial Phagocytosis and Its Regulation: A Therapeutic Target in Parkinson's Disease? Front Mol Neurosci. 2018;11:144.
18. Gabande-Rodriguez E, Keane L, Capasso M. Microglial phagocytosis in aging and Alzheimer's disease. J Neurosci Res. 2020;98(2):284-98.
19. Joshi T, Butchar JP, Tridandapani S. Fcgamma receptor signaling in phagocytes. Int J Hematol. 2006;84(3):210-6.
20. Lee HJ, Woo Y, Hahn TW, Jung YM, Jung YJ. Formation and Maturation of the Phagosome: A Key Mechanism in Innate Immunity against Intracellular Bacterial Infection. Microorganisms. 2020;8(9).
21. Galloway DA, Phillips AEM, Owen DRJ, Moore CS. Corrigendum: Phagocytosis in the

Brain: Homeostasis and Disease. Front Immunol. 2019;10:1575.
22. Joshi T, Butchar JP, Tridandapani S. Fcgamma Receptor Signaling in Phagocytes. Int J Hematol. 2006;84(3):210-6.
23. Tohyama Y, Yamamura H. Complement-mediated phagocytosis--the role of Syk. IUBMB Life. 2006;58(5-6):304-8.
24. Spiering D, Hodgson L. Dynamics of the Rho-family small GTPases in actin regulation and motility. Cell Adh Migr. 2011;5(2):170-80.
25. Botelho RJ, Grinstein S. Phagocytosis. Curr Biol. 2011;21(14):R533-8.
26. Jaumouille V, Waterman CM. Physical Constraints and Forces Involved in Phagocytosis. Front Immunol. 2020;11:1097.
27. Lafuente EM, Niedergang F, Rosales C. Editorial: Phagocytosis: Molecular Mechanisms and Physiological Implications. Front Immunol. 2020;11:586918.
28. Araki N. Role of microtubules and myosins in Fc gamma receptor-mediated phagocytosis. Front Biosci. 2006;11:1479-90.
29. Chakraborty R, Goswami C. Both heat-sensitive TRPV4 and cold-sensitive TRPM8 ion channels regulate microglial activity. Biochemical and Biophysical Research Communications. 2022;611:132-9.
30. Umpierre AD, Bystrom LL, Ying Y, Liu YU, Worrell G, Wu LJ. Microglial calcium signaling is attuned to neuronal activity in awake mice. Elife. 2020;9.
31. Redmon SN, Yarishkin O, Lakk M, Jo A, Mustafic E, Tvrdik P, et al. TRPV4 channels mediate the mechanoresponse in retinal microglia. Glia. 2021;69(6):1563-82.
32. Furnish M, Caino MC. Altered mitochondrial trafficking as a novel mechanism of cancer metastasis. Cancer Rep (Hoboken). 2020;3(1):e1157.
33. Vasek MJ, Deajon-Jackson JD, Liu Y, Crosby HW, Yi J, Dougherty JD. Microglia perform local protein synthesis at perisynaptic and phagocytic structures. bioRxiv. 2021:2021.01.13.426577.
34. Echeverry S, Rodriguez MJ, Torres YP. Transient Receptor Potential Channels in Microglia: Roles in Physiology and Disease. Neurotox Res. 2016;30(3):467-78.
35. Annesley SJ, Fisher PR. Mitochondria in Health and Disease. Cells. 2019;8(7).
36. McAvoy K, Kawamata H. Glial mitochondrial function and dysfunction in health and neurodegeneration. Mol Cell Neurosci. 2019;101:103417.
37. Zhou Z, Austin GL, Young LEA, Johnson LA, Sun R. Mitochondrial Metabolism in Major Neurological Diseases. Cells. 2018;7(12).
38. Nunnari J, Suomalainen A. Mitochondria: in sickness and in health. Cell. 2012;148(6):1145-59.
39. Bravo-Sagua R, Parra V, Lopez-Crisosto C, Diaz P, Quest AF, Lavandero S. Calcium Transport and Signaling in Mitochondria. Compr Physiol. 2017;7(2):623-34.
40. Frederick RL, Shaw JM. Moving mitochondria: establishing distribution of an essential organelle. Traffic. 2007;8(12):1668-75.
41. Lovas JR, Wang X. The meaning of mitochondrial movement to a neuron's life. Biochim Biophys Acta. 2013;1833(1):184-94.
42. Sato O, Sakai T, Choo YY, Ikebe R, Watanabe TM, Ikebe M. Mitochondria-associated myosin 19 processively transports mitochondria on actin tracks in living cells. J Biol Chem. 2022;298(5):101883.
43. Adebayo M, Singh S, Singh AP, Dasgupta S. Mitochondrial fusion and fission: The fine-tune balance for cellular homeostasis. FASEB J. 2021;35(6):e21620.
44. Li Y, Xia X, Wang Y, Zheng JC. Mitochondrial dysfunction in microglia: a novel perspective for pathogenesis of Alzheimer's disease. J Neuroinflammation. 2022;19(1):248.
45. Rangaraju V, Lewis TL, Jr., Hirabayashi Y, Bergami M, Motori E, Cartoni R, et al. Pleiotropic Mitochondria: The Influence of Mitochondria on Neuronal Development and Disease. J Neurosci. 2019;39(42):8200-8.
46. Trigo D, Avelar C, Fernandes M, Sa J, da Cruz ESO. Mitochondria, energy, and metabolism in neuronal health and disease. FEBS Lett. 2022;596(9):1095-110.
47. Nakaso K. Roles of Microglia in Neurodegenerative Diseases. Yonago Acta Med. 2024;67(1):1-8.
48. Beeken J, Mertens M, Stas N, Kessels S, Aerts L, Janssen B, et al. Acute inhibition of transient receptor potential vanilloid-type 4 cation channel halts cytoskeletal dynamism in microglia. Glia. 2022;70(11):2157-68.

49. Wang X, Schwarz TL. The mechanism of Ca2+ -dependent regulation of kinesin-mediated mitochondrial motility. Cell. 2009;136(1):163-74.
50. Goswami C, Kuhn J, Heppenstall PA, Hucho T. Importance of non-selective cation channel TRPV4 interaction with cytoskeleton and their reciprocal regulations in cultured cells. PLoS One. 2010;5(7):e11654.
51. Li Y, Li T, Chen T, Li C, Yu W, Xu Y, et al. The Role of Microglia with Mitochondrial Dysfunction and Its Therapeutic Prospects in Alzheimer's Disease. J Integr Neurosci. 2024;23(5):91.
52. Zamponi N, Zamponi E, Cannas SA, Billoni OV, Helguera PR, Chialvo DR. Mitochondrial network complexity emerges from fission/fusion dynamics. Sci Rep. 2018;8(1):363.
53. Al Ojaimi M, Salah A, El-Hattab AW. Mitochondrial Fission and Fusion: Molecular Mechanisms, Biological Functions, and Related Disorders. Membranes (Basel). 2022;12(9).
54. Scott I, Youle RJ. Mitochondrial fission and fusion. Essays Biochem. 2010;47:85-98.
55. Acharya TK, Kumar A, Kumar S, Goswami C. TRPV4 interacts with MFN2 and facilitates endoplasmic reticulum-mitochondrial contact points for Ca(2+)-buffering. Life Sci. 2022;310:121112.
56. Ding WX, Yin XM. Mitophagy: mechanisms, pathophysiological roles, and analysis. Biol Chem. 2012;393(7):547-64.
57. Xue C, Gong J, Guo Y, Yin J, He X, Huang H, et al. Oxygenized low density lipoprotein down-regulates the TRPV4 protein expression of macrophage through activation of peroxisome proliferator-activated receptor gamma. Minerva Med. 2017;108(1):1-12.
58. Holloman JP, Dimas SH, Archambault AS, Filipello F, Du L, Feng J, et al. Transient Receptor Potential Vanilloid 4-Dependent Microglial Function in Myelin Injury and Repair. Int J Mol Sci. 2023;24(23).
59. Jin M, Wu Z, Chen L, Jaimes J, Collins D, Walters ET, et al. Determinants of TRPV4 activity following selective activation by small molecule agonist GSK1016790A. PLoS One. 2011;6(2):e16713.
60. Macaskill AF, Rinholm JE, Twelvetrees AE, Arancibia-Carcamo IL, Muir J, Fransson A, et al. Miro1 is a calcium sensor for glutamate receptor-dependent localization of mitochondria at synapses. Neuron. 2009;61(4):541-55.
61. Lefebvre A, Ma D, Kessenbrock K, Lawson DA, Digman MA. Author Correction: Automated segmentation and tracking of mitochondria in live-cell time-lapse images. Nat Methods. 2022;19(6):770.
62. Chakraborty R, Nonaka T, Hasegawa M, Zurzolo C. Tunnelling nanotubes between neuronal and microglial cells allow bi-directional transfer of alpha-Synuclein and mitochondria. Cell Death Dis. 2023;14(5):329.
63. Agrawal I, Jha S. Mitochondrial Dysfunction and Alzheimer's Disease: Role of Microglia. Front Aging Neurosci. 2020;12:252.
64. Peggion C, Cali T, Brini M. Mitochondria Dysfunction and Neuroinflammation in Neurodegeneration: Who Comes First? Antioxidants (Basel). 2024;13(2).
65. Morton H, Kshirsagar S, Orlov E, Bunquin LE, Sawant N, Boleng L, et al. Defective mitophagy and synaptic degeneration in Alzheimer's disease: Focus on aging, mitochondria and synapse. Free Radic Biol Med. 2021;172:652-67.
66. Fairley LH, Wong JH, Barron AM. Mitochondrial Regulation of Microglial Immunometabolism in Alzheimer's Disease. Front Immunol. 2021;12:624538.

Acknowledgements – Schellingen R is grateful for the opportunity to collaborate to the research of PhD candidate Burlacu A under the guidance of Brône B, acknowledging the funding provided by the Bijzonder Onderzoeksfonds (BOF). Schellingen R wishes to thank Burlacu A, Trippaers C, Mertens M, Zaghbouni S and Cornelissen F for the assistance during the internship. Schellingen R acknowledges the Advanced Optical Microscopy Centre at Hasselt University for support with the microscopy experiments. Microscopy was made possible by (1) the Research Foundation Flanders (FWO, project G0H3716N) - Zeiss LSM880, (2) the Research Foundation Flanders (FWO, project I001222N) - Zeiss LSM900. Duwé S is gratefully acknowledged for his knowledge and guidance with the microscopy experiments.

Author contributions –Burlacu A and Alpizar Y.A. designed the research under the responsibility of Brône B. Burlacu A and Schellingen R contributed equally to the experiments, data collection, and data analysis. Schellingen R wrote the paper under the guidance of Burlacu A.

SUPPLEMENTARY MATERIALS

Culture of RAW264.7 – RAW 264.7 cells (19th passage) were cultured in DMEM F12 medium supplemented with 10% Fetal Calf Serum (FCS) and 1% L-glutamine and maintained in an incubator at 37°C with 5% CO_2. Cells were passaged after reaching 90% confluence, detached with a cell scraper and subcultured in 1:6 ratio in T-175 flasks.

Suppl. Table 1: primer sequences for PCR	
TRPV4	
F1	5' - GCT CCT GTT GAA CAT GCT TAT CG - 3'
F2	5' - CAT GAA ATC TGA CCT CTT GTC CCC - 3'
R1	5' - CTG TCC CAG CCT CCC CTC CT -3'
CX3CR1	
F1	5' - GTC TTC ACG TTC GGT CTG GT -3'
F3	5' - CTC CCC CTG AAC CTG AAA C - 3'
R1	5' - CCC AGA CAC TCG TTG TCC TT -3'
F1 = WT forward primer F2 = KO forward primer F3= mutant forward primer R1 = Reverse primer	

Suppl. Table 2: Mitochondrial parameters used in mitochondrial network analysis.	
Total branch length	Sum of the length of all branches present in the image.
Mean branch length	The total branch length divided by the number of branches.
Number of mitochondria	Number of mitochondria present in the image.
Number of mitochondrial branches	Total number of branches present in the image.
Total surface area	Sum of the surface area of all mitochondria in the image
Mean surface area	Total surface area divided by the number of mitochondria
Branch junctions	The number of junctions within all skeletons in the image. A junction is a point where 2 or more branches meet.
Branch end points	The total number of end points, which is where a branch ends without connecting to another branch.

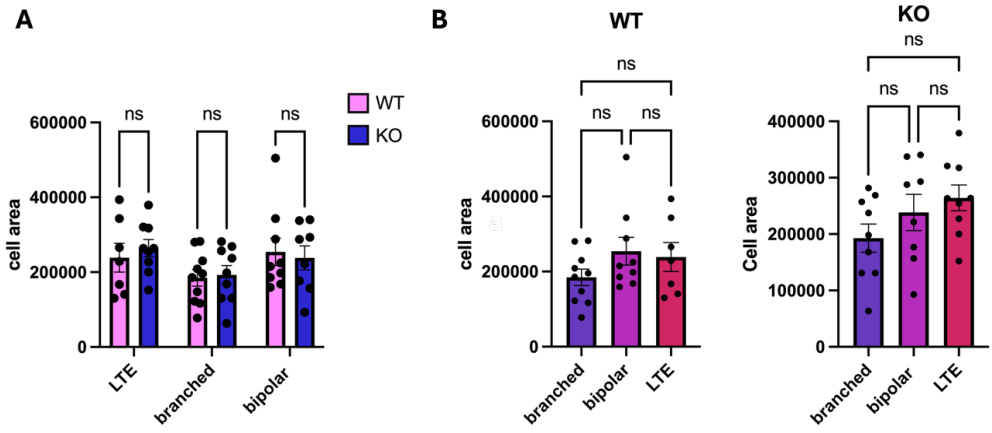

Supplemental Figure 1: No differences in cell area were found between WT and KO microglia. Cell area was measured using the binary eGFP signal of each cell in Fiji ImageJ. Three distinct phenotypes were chosen: (1) branched microglia, (2) bipolar microglia, and (3) microglia with a lamellipodium and a trailing edge (LTE). **(A)** Quantification of the difference in cell area for WT and KO microglia. No significant difference was observed. **(B)** Quantification of the difference in cell area for different phenotypes in WT and KO microglia. No significant differences in cell size were observed between phenotypes. Analysis was performed for each phenotype in WT (n_B= 9, n_{LTE}= 7, n_{bip}= 9) and KO microglia (n_B= 9, n_{LTE} = 9, n_{bip}= 8). Normality was checked using the Shapiro-Wilk test. Statistical significance was assessed using a two-way anova to compare WT vs KO, a one-way anova for normally distributed data, or the Kruskal-Wallis test for not normally distributed data to compare between phenotypes (*p <0.05). Data represent mean ±SEM.
WT = wild-type, KO= knockout, eGFP= enhanced green fluorescent protein, B= branched, bip= bipolar, ns= non-significant.

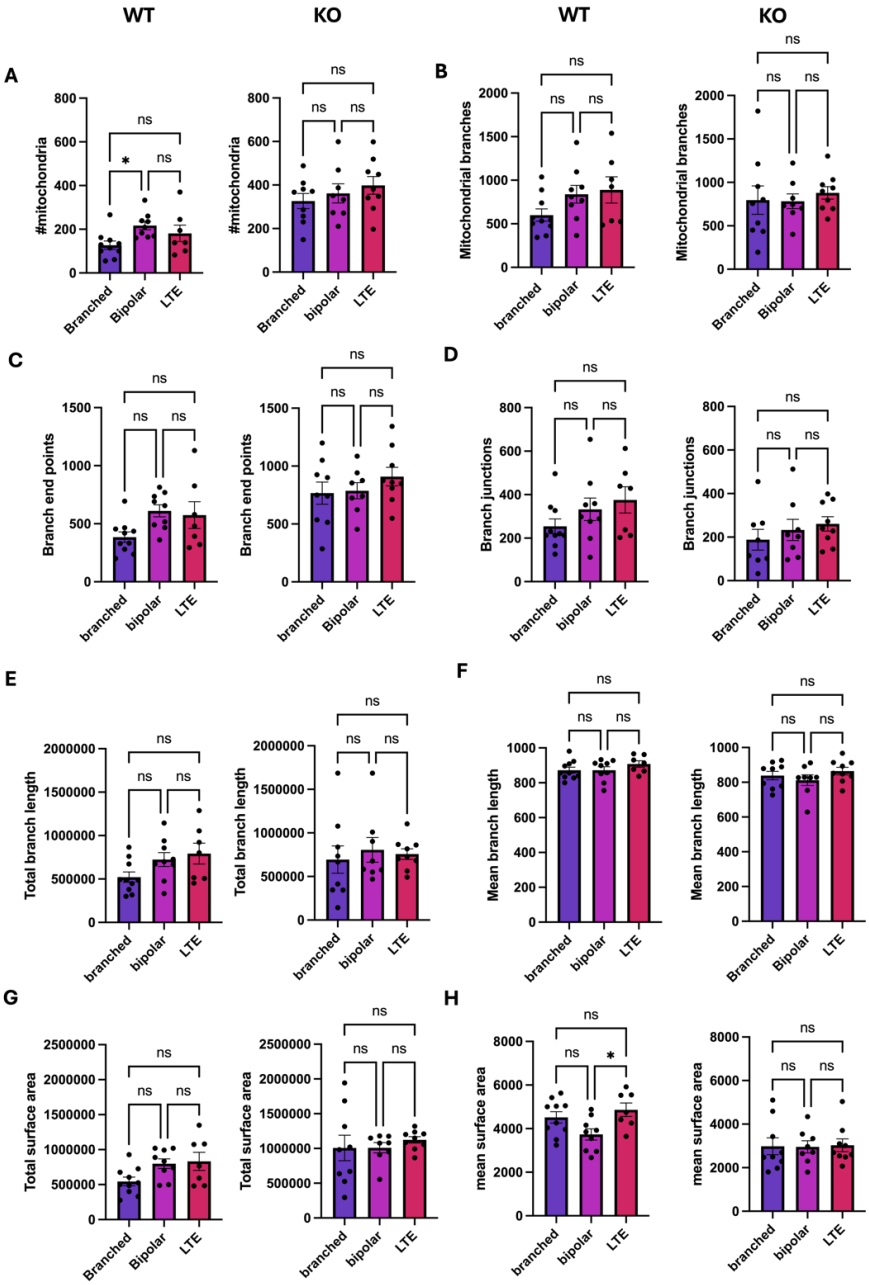

Supplemental Figure 2: Mitochondrial analysis between phenotypes in WT and KO microglia. Mitochondrial network analysis was performed using Mitochondrial Analyzer in Fiji ImageJ. Three distinct phenotypes were chosen: (1) branched microglia, (2) bipolar microglia, and (3) microglia with a lamellipodium and a trailing edge (LTE). **(A)** Quantification of number of mitochondria present in each phenotype for WT and KO microglia. **(B)** Quantification of the number of mitochondrial branches. **(C)** Quantification of the branch end points. **(D)** number of branch junctions. **(E)** Total mitochondrial branch length. **(F)** mean mitochondrial branch length. **(G)** Total surface area. **(H)** Mean surface area. Analysis was performed for each phenotype in WT (n_B= 9, n_{LTE}= 7, n_{bip}= 9) and KO microglia (n_B= 9, n_{LTE} = 9, n_{bip}= 8). Normality was checked using the Shapiro-Wilk test. Statistical significance was assessed using a one-way anova for normally distributed data, or the Kruskal-Wallis test for not normally distributed data (*p <0.05) Data represent mean ±SEM.

WT = wild-type, KO= knockout, eGFP= enhanced green fluorescent protein, B= branched, bip= bipolar, ns= non-significant.

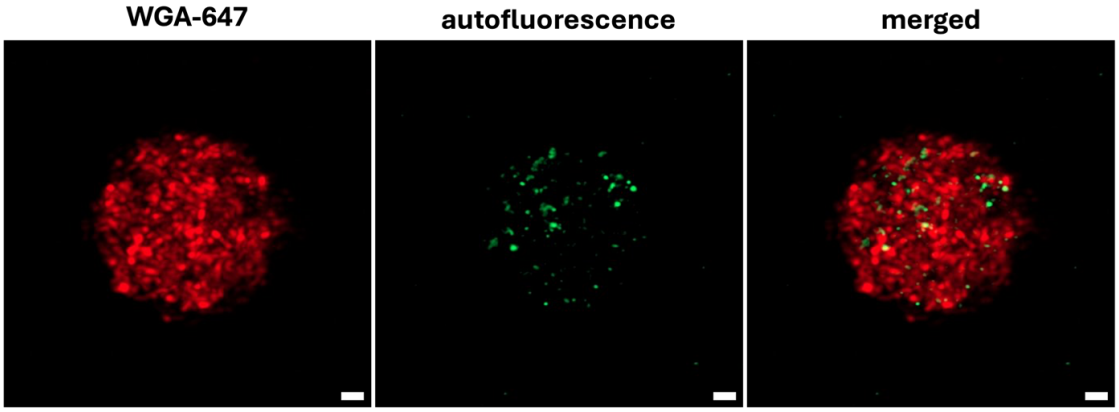

Supplemental figure 3: green autofluorescence in RAW264.7 cells. The membrane of RAW264.7 was stained with WGA-647 (red). Green autofluorescence was checked on the LSM900. Scalebar represents 1 µm.
WGA= wheat germ agglutin

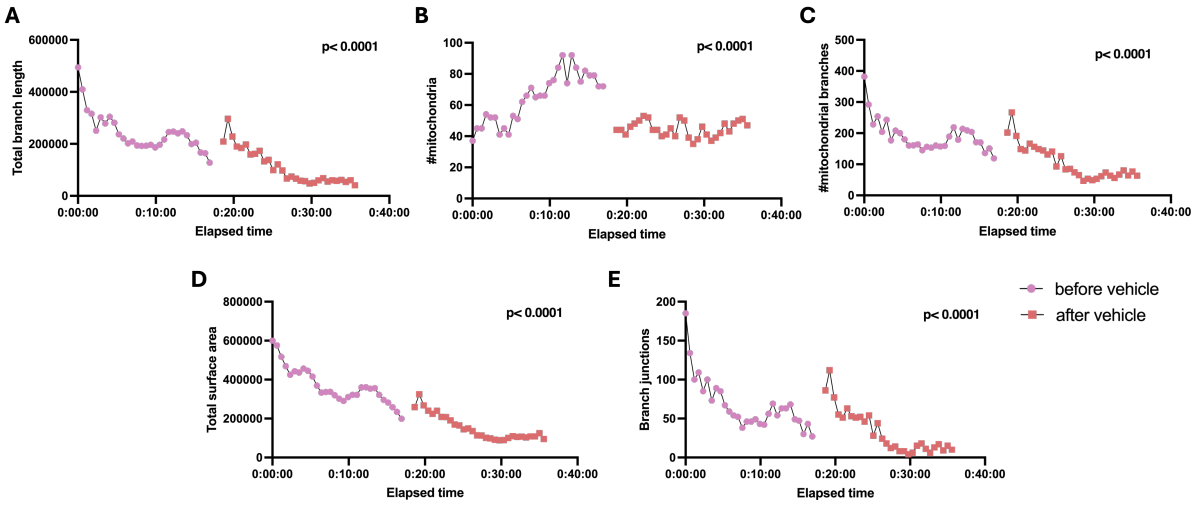

Supplemental figure 4: Mitochondrial analysis before and after administration of the vehicle. MilliQ was used as a vehicle control. **(A-E)** Quantification of mitochondrial parameters; difference in total branch length **(A)**, number of mitochondria **(B)**, number of mitochondrial branches **(C)**, number of branch junctions **(D)**, and total surface area **(E)** (n = 1). Statistical significance was assessed using the Mann-Whitney test *p <0.05, **p<0,01, ***p<0,001, ****p<0,0001). Data represent mean ±SEM.

.

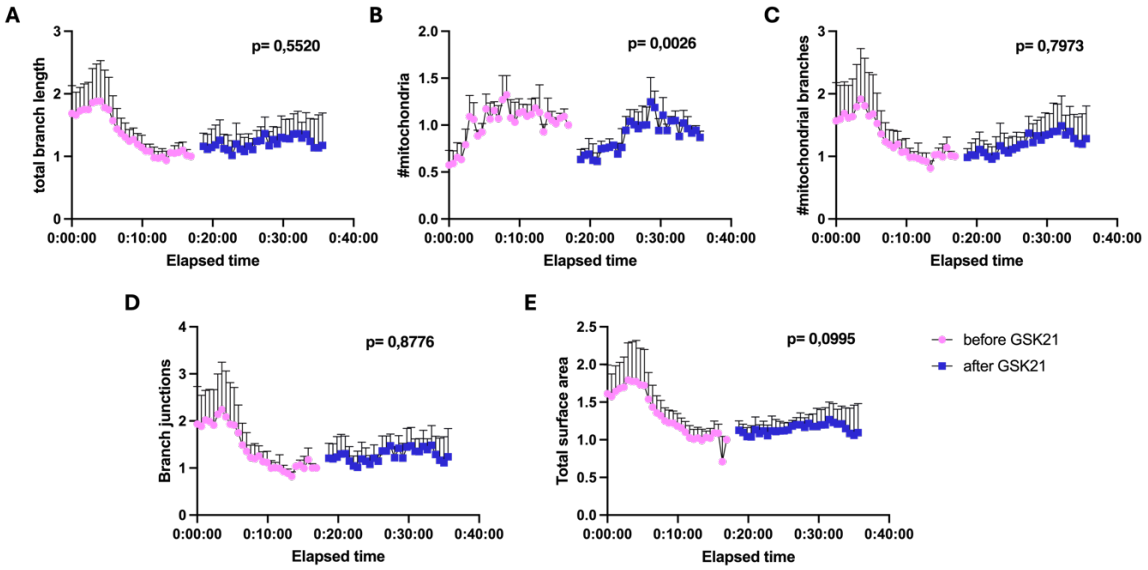

Supplemental figure 5: Mitochondrial analysis before and after administration of GSK21. Mitochondrial network analysis in WT microglia **(A-E)** Quantification of mitochondrial parameters; difference in total branch length **(A)**, number of mitochondria **(B)**, number of mitochondrial branches **(C)**, number of branch junctions **(D)**, and total surface area **(E)** (n = 3). Statistical significance was assessed using the Mann-Whitney test *p <0.05, **p<0,01, ***p<0,001, ****p<0,0001). Data represent mean ±SEM.
WT = wild-type, eGFP= enhanced green fluorescent protein, TRPV4= transient receptor potential vanilloid 4.